Article

Cancer Cell

Ripretinib (DCC-2618) Is a Switch Control Kinase Inhibitor of a Broad Spectrum of Oncogenic and Drug-Resistant KIT and PDGFRA Variants

Highlights

- Ripretinib broadly inhibits primary and drug-resistant KIT/PDGFRA mutants
- KIT/PDGFRA inhibitor of all known activation loop mutations
- In drug-resistant cancers, ripretinib blocks kinase signaling and tumor growth
- Circulating tumor DNA data confirm broad inhibition of mutant KIT in GIST patients

Authors

Bryan D. Smith, Michael D. Kaufman, Wei-Ping Lu, ..., Oliver Rosen, Michael C. Heinrich, Daniel L. Flynn

Correspondence

dflynn@deciphera.com

In Brief

To overcome the often multi-subclonal mutations in treatment-resistant GIST, Smith et al. design ripretinib, which targets a broad spectrum of KIT and PDGFRA mutants. Ripretinib shows efficacy in KIT and PDGFRA mutant cancer models and reduces circulating tumor DNA mutant allele frequency in two GIST patients.

Smith et al., 2019, Cancer Cell *35*, 738–751
May 13, 2019
https://doi.org/10.1016/j.ccell.2019.04.006

CellPress

CellPress

Cancer Cell
Article

Ripretinib (DCC-2618) Is a Switch Control Kinase Inhibitor of a Broad Spectrum of Oncogenic and Drug-Resistant KIT and PDGFRA Variants

Bryan D. Smith,[1] Michael D. Kaufman,[1] Wei-Ping Lu,[1] Anu Gupta,[1] Cynthia B. Leary,[1] Scott C. Wise,[1,6] Thomas J. Rutkoski,[1] Yu Mi Ahn,[1] Gada Al-Ani,[1] Stacie L. Bulfer,[1] Timothy M. Caldwell,[1] Lawrence Chun,[2] Carol L. Ensinger,[1] Molly M. Hood,[1] Arin McKinley,[5] William C. Patt,[1] Rodrigo Ruiz-Soto,[1] Ying Su,[1] Hanumaiah Telikepalli,[1] Ajia Town,[5] Benjamin A. Turner,[1] Lakshminarayana Vogeti,[1] Subha Vogeti,[1] Karen Yates,[1] Filip Janku,[3] Albiruni Ryan Abdul Razak,[4] Oliver Rosen,[1] Michael C. Heinrich,[5] and Daniel L. Flynn[1,7,*]

[1]Deciphera Pharmaceuticals, Inc., Waltham, MA 02451, USA
[2]Emerald Biostructures, Bainbridge Island, WA 98110, USA
[3]The University of Texas MD Anderson Cancer Center, Department of Investigational Cancer Therapeutics, Houston, TX 77030, USA
[4]Princess Margaret Cancer Centre, Cancer Clinical Research Unit, Toronto, ON, Canada
[5]Portland VA Medical Center and Oregon Health & Science University Knight Cancer Institute, Portland, OR 97239, USA
[6]Present address: MI Bioresearch, Ann Arbor, MI 48108, USA
[7]Lead Contact
*Correspondence: dflynn@deciphera.com
https://doi.org/10.1016/j.ccell.2019.04.006

SUMMARY

Ripretinib (DCC-2618) was designed to inhibit the full spectrum of mutant KIT and PDGFRA kinases found in cancers and myeloproliferative neoplasms, particularly in gastrointestinal stromal tumors (GISTs), in which the heterogeneity of drug-resistant KIT mutations is a major challenge. Ripretinib is a "switch-control" kinase inhibitor that forces the activation loop (or activation "switch") into an inactive conformation. Ripretinib inhibits all tested KIT and PDGFRA mutants, and notably is a type II kinase inhibitor demonstrated to broadly inhibit activation loop mutations in KIT and PDGFRA, previously thought only achievable with type I inhibitors. Ripretinib shows efficacy in preclinical cancer models, and preliminary clinical data provide proof-of-concept that ripretinib inhibits a wide range of KIT mutants in patients with drug-resistant GISTs.

INTRODUCTION

Activating mutations and other genetic alterations in *KIT* and *PDGFRA* receptor tyrosine kinases have been identified in many cancers and myeloproliferative diseases (Beadling et al., 2008; Heinrich et al., 2003a; Kemmer et al., 2004; Malaise et al., 2009; Verstovsek, 2013). Gastrointestinal stromal tumors (GISTs) are driven by activating mutations in KIT (~80%) and the related PDGFRA (~5%–10%) receptor tyrosine kinases (Corless et al., 2011; Heinrich et al., 2003a). Mutations in *KIT* drive >90% of cases of systemic mastocytosis (SM) and mast cell leukemia (MCL) (Arock et al., 2015), and small but significant percentages of acute myeloid leukemia (AML), germ cell tumors, and melanoma (Beadling et al., 2008; Kemmer et al., 2004; Malaise et al., 2009). *PDGFRA* mutations or gene rearrangements are observed in cancers such as hypereosinophilic leukemia and glioblastoma (Brennan et al., 2013; Cools et al., 2003). *KIT* and/or *PDGFRA* gene amplifications are likely oncogenic in gliomas and lung cancers (Brennan et al., 2013; Joensuu et al., 2005; Ramos et al., 2009; Verhaak et al., 2010).

Approximately 10% of GISTs have primary mutations in KIT within the extracellular domain (encoded by exon 9). Mutations in this domain cause ligand-independent receptor dimerization and activation (Corless et al., 2011). Aside from these exon 9 mutations, the vast majority of primary and secondary resistance mutations in KIT and PDGFRA are located within

Significance

Genetic alterations in *KIT* or *PDGFRA* kinase are detected in >85% of cases of GIST and systemic mastocytosis, as well as in small but significant percentages of AML, melanoma, germ cell tumors, lung cancer, and glioblastoma. FDA-approved KIT kinase inhibitors have transformed the treatment of GIST. However, resistance mutations inevitably emerge during therapy, causing disease progression. Most resistance mutations in GIST occur within KIT, yet are quite heterogeneous, with most patients acquiring multiple subclonal mutations. An inhibitor that blocks only a subset of resistance mutations allows for the growth of other resistant subclones. As a result, in GIST there is an unmet medical need for a drug that comprehensively inhibits KIT and PDGFRA mutants.

conformation-controlling switch regions embedded in the intracellular kinase domain. KIT and PDGFRA are dual-switch kinases (Mol et al., 2004), each containing (1) an inhibitory switch in the intracellular juxtamembrane domain (JMD) region encoded by *KIT* exon 11 or *PDGFRA* exon 12, and (2) a main activation loop (AL) switch within the kinase domain encoded by *KIT* exons 17 and 18 or *PDGFRA* exons 18 and 19. This dual-switch mechanism carefully regulates cellular kinase activity by control of kinase conformation. Mechanistically, switch control of kinase conformation is mediated by phosphorylation of one or more switch amino acids that turn the kinase "on" or "off" (Huse and Kuriyan, 2002). Oncogenic kinase mutations predominantly function by disrupting one or more regulatory switch mechanisms, leading to dysregulated switch function and loss of physiologic conformational control (Blume-Jensen and Hunter, 2001; Chan et al., 2011; Klug et al., 2018). In approximately 70% of GIST patients, the primary activating mutation is found in the KIT exon 11 JMD inhibitory switch (Rubin et al., 2001). Tyrosine phosphorylation or mutations in this switch disrupt the inactive type II form of KIT, leading to a shift in the conformational equilibrium toward a type I active form. A small percentage of primary activating mutations and virtually all secondary resistance mutations in GIST are located either in the main AL switch (encoded by *KIT* exons 17 and 18; *PDGFRA* exon 18) or in the cognate switch pocket (including *KIT* exons 13/14 or *PDGFRA* exons 14/15). These activating mutations stabilize the active type I conformation. In particular, the exon 17 D816 switch residue of KIT and the analogous exon 18 D842 residue of PDGFRA are essential for the AL switches to reside in a type II off state, and their mutation to valine leads to disruption of this type II state, leading to a type I active state (Gajiwala et al., 2009). Mast cell diseases, such as SM and MCL, and small percentages of AML, are driven by primary mutations, such as D816V or N822K, in the main AL switch of KIT (Paschka et al., 2006). Similarly, a D842V mutation within the PDGFRA main AL switch is the most common primary mutation observed within the small subset of PDGFRA mutant GIST (Heinrich et al., 2003b).

Treatment of metastatic or unresectable GIST has been transformed by kinase inhibitors, beginning with the realization that imatinib exhibited KIT inhibition (Heinrich et al., 2000; Joensuu et al., 2001). Imatinib, as well as two other multi-targeted KIT and PDGFRA kinase inhibitors, sunitinib and regorafenib, are US Food and Drug Administration (FDA)-approved treatments for GIST (Serrano and George, 2014). Currently available treatment options offer modest clinical benefit after patients have progressed on imatinib with a median progression-free survival not exceeding 6 months for sunitinib and regorafenib (Demetri et al., 2006, 2013). Imatinib and regorafenib are type II kinase inhibitors and bind to the inactive conformations of KIT and PDGFRA. Sunitinib, despite binding some kinases in a type I conformation, is a type II inhibitor of KIT (DiNitto et al., 2010; Gajiwala et al., 2009). These three FDA-approved type II KIT inhibitors block a limited number of activating KIT mutants. Although the conformational equilibrium in primary KIT mutants (mutations in exon 11 JMD inhibitory switch) is shifted toward the type I active conformation, these inhibitors can nonetheless bind and stabilize KIT in the inactive type II conformation. However, for many activating KIT or PDGFRA mutations that more prominently shift equilibrium to the activated type I conformation, identifying effective type II inhibitors has remained elusive (Blay, 2011; Evans et al., 2017; Gajiwala et al., 2009; Gounder and Maki, 2011; Heinrich et al., 2006). The KIT exon 17 AL switch mutation D816V drives a large majority of cases of SM and MCL (Bibi et al., 2014; Nagata et al., 1995), and many other exon 17 or 18 mutations occur in acquired GIST resistance (Corless et al., 2011; Liegl et al., 2008). In addition, the PDGFRA exon 18 AL switch mutation D842V is causative of ~5%–10% of primary GIST (Heinrich et al., 2003b). Midostaurin and BLU-285 are type I inhibitors that block a subset of AL mutations in KIT or PDGFRA. Notably, it has been recently reported that these aggressive AL mutations can only be inhibited by type I, but not type II, inhibitors (Evans et al., 2017). Midostaurin has recently received FDA approval for treatment of SM (Gotlib et al., 2016; Peter et al., 2016), and BLU-285 is in clinical development for both SM and GIST (Evans et al., 2017). However, these type I inhibitors only block a subset of clinically relevant mutations.

Given the heterogeneous nature of KIT and PDGFRA mutants in GIST, it is desirable to use a treatment that inhibits as many mutants as possible, to both block the various simultaneous mutations that are present in imatinib-resistant metastatic GIST patients, as well as to limit the disease impact of further resistance mutations that may arise. Using our switch control inhibitor platform (Ahn et al., 2010; Chan et al., 2011; Harney et al., 2017), we designed a KIT and PDGFRA inhibitor that broadly inhibits activating mutations spanning all relevant known exons, including AL mutations previously believed to be targeted only by type I inhibitors.

RESULTS

X-Ray Co-crystal Structural Correlates of KIT Switch Control Inhibition

Ripretinib (Figure 1A) was synthesized as described in US patent 8461179B1, example 31. Analysis of the X-ray co-crystal structure of KIT kinase with a close chloro analog, DP-2976 (Figure 1A), is shown in Figures 1B–1E (PDB: 6MOB). The co-crystal structure of DP-2976 with KIT reveals key elements of switch control inhibition. First, the terminal phenyl ring of DP-2976 is shown to occupy the third position (magenta) in the vertical interior hydrophobic cluster (R-spine) within the switch pocket, providing a surrogate for the missing tryptophan from the deleted/mutated KIT exon 11 inhibitory JMD switch that would have otherwise occupied this position (compare Figure 1B with Figure S1A). Mutations in the analogous JMD inhibitory switch exist in PDGFRA (Figure S1B). The inhibitor phenyl ring thus completes a vertical cluster of hydrophobic amino acids also comprising L656, L644, and H790 to maintain the inhibitory R-spine (Hu et al., 2015). This region is also comprised of additional amino acids (V643, L647, I653, V654, L783, H790, and I808) that physiologically accept and stabilize the AL switch phenyl side chain of F811 (DFG motif) in a type I active state. Direct occupancy of this region by DP-2976 antagonizes the AL switch (Figure 1C). Additional hydrophobic interactions exist between the chloro substituent of the central phenyl ring and V603, A621, K623, and T670. In composite, these hydrophobic

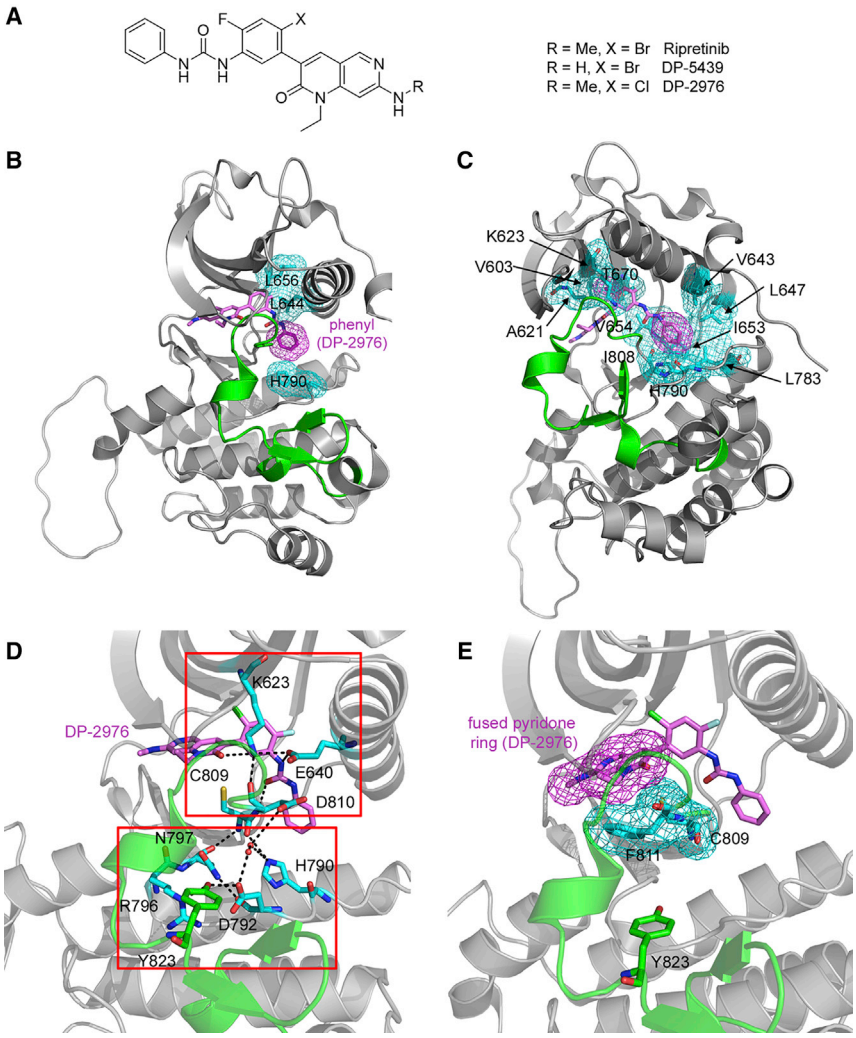

Figure 1. Chemical Structure of Ripretinib (DCC-2618) and X-Ray Crystal Structure of Analog DP-2976 Bound to KIT

(A) Chemical structures of ripretinib, active metabolite DP-5439, and analog DP-2976.

(B) Phenyl ring of DP-2976 occupies the switch pocket region as a surrogate for the JMD inhibitory switch tryptophan.

(C) Surface representation of hydrophobic interactions in switch pocket regions by DP-2976.

(D) Hydrogen bond network that stabilizes Y823 as a decoy substrate. The upper red box highlights direct hydrogen bond interactions of DP-2976 with key switch residues K623, E640, and D810. The lower red box highlights an extended hydrogen bond network nucleated by inhibitor binding, maintaining a pocket for binding decoy substrate AL switch residue Y823.

(E) Electronic and hydrophobic interactions of inhibitor with switch residues C809 and F811. The coordinates of the crystal structure are deposited with the protein databank (PDB: 6MOB).

See also Figure S1 and Table S1.

interactions antagonize occupancy of the AL switch type I active state (Figure S1C). In addition to these hydrophobic interactions, DP-2976 also forms key hydrogen bonds that control AL switch conformation. The fused pyridone carbonyl oxygen and the inhibitor urea moiety form a network of four hydrogen bonds with switch amino acids K623, E640, and D810. These hydrogen bond interactions also serve an antagonist role, displacing the AL switch into an inactive type II state (Figure 1D, upper red box). These hydrogen bonds further nucleate additional hydrogen bonds that comprise the catalytic amino acids H790, D792, R796, N797, and C809. This nucleation of multiple hydrogen bonds maintains a pocket for stabilizing the AL switch in the inactive type II state, binding the switch residue Y823 as a decoy substrate. This extended hydrogen bond network and stabilization of the pocket for Y823 provides an agonist function to favor the AL switch type II inactive state (Figure 1D, bottom red box). Finally, the fused pyridone ring of DP-2976 forms extensive hydrophobic and van der Waals interactions with switch amino acids C809 and F811, providing an agonist function for further maintaining the AL switch in a type II inactive state (Figure 1E). In summary, the switch control design concepts that were incorporated into ripretinib both antagonize the switches from adopting a type I active state, and stabilize (agonize) switch elements in the type II inactive state (Ahn et al., 2010; Chan et al., 2011; Harney et al., 2017). Data collection and refinement statistics are shown in Table S1.

Ripretinib Is a Potent Inhibitor of Mutant KIT and PDGFRA Kinases *In Vitro*

In vitro kinase inhibition studies demonstrate that ripretinib is a potent inhibitor of wild-type (WT) KIT and PDGFRA, and oncogenic and drug-resistant variants (Table 1). DP-5439 (Figure 1A; an abundant active metabolite of ripretinib identified in preclinical and clinical studies; our unpublished data), DP-2976 (Figure 1A; chloro analog of ripretinib), imatinib, sunitinib, and regorafenib are type II inhibitors of KIT and PDGFRA, whereas midostaurin and BLU-285 are type I inhibitors shown for comparison. Most kinase inhibitors are sensitive to ATP concentration; thus, assays were performed at approximate cellular levels of ATP (1 mM) to reflect physiologic conditions. Data showing the resiliency of ripretinib and DP-5439 up to 4 mM ATP concentration is shown in Figure S2A.

KIT kinase exists in at least three stable conformations, including an unphosphorylated autoinhibited state, an active form wherein two key tyrosine residues in the JMD are phosphorylated, and a fully phosphorylated active conformation wherein Y823 in the AL is additionally phosphorylated (DiNitto et al., 2010; Wodicka et al., 2010). In kinase activity assays, the latter two forms were assessed. Type II inhibitors imatinib, sunitinib, and regorafenib favor the JMD phosphorylated form over the fully phosphorylated form of KIT by >30- to 1,000-fold, reflecting their higher potency for KIT forms presenting a higher proportional population of the type II state. The lower potency of these compounds versus the fully phosphorylated type I KIT state

Table 1. *In Vitro* Inhibition of Recombinant KIT and PDGFRA Kinases by Type I and Type II Inhibitors

	Inhibitor Type	JMD Phosphorylated WT KIT	Fully Phosphorylated WT KIT	KIT V654A Exon 13	KIT T670I Exon 14	KIT D816H Exon 17	KIT D816V Exon 17	PDGFRA WT	PDGFRA D842V Exon 18
		IC_{50} (nM)							
Ripretinib	Type II	3.0 ± 0.5	13 ± 8	11 ± 6	9.2 ± 1.1	18 ± 4	25 ± 9	3.6 ± 1.0	36 ± 8
DP-5439	Type II	2.9 ± 1.0	15 ± 7	11 ± 4	3.4 ± 1.8	15 ± 4	19 ± 6	3.4 ± 1.0	42 ± 19
DP-2976	Type II	2.7 ± 0.6	7 ± 4	28 ± 3	2.7 ± 0.5	33 ± 16	11 ± 1	1.8 ± 0.1	32 ± 10
Imatinib	Type II	66 ± 10	>3,300	>3,300	>3,300	>3,300	>3,300	28 ± 6	270 ± 80
Sunitinib	Type II	2.9 ± 0.5	>3,300	8.1 ± 1.0	1.3 ± 0.6	>3,300	2,800 ± 900	3.0 ± 0.6	550 ± 130
Regorafenib	Type II	4.4 ± 0.5	130 ± 40	17 ± 8	2.6 ± 0.7	1,450 ± 140	>3,300	2.7 ± 0.3	35 ± 30
Midostaurin	Type I	118 ± 10	220 ± 105	>3,300	10.4 ± 2.5	23 ± 2	15 ± 3	35 ± 2	38 ± 4
BLU-285	Type I	24 ± 1	96 ± 83	660 ± 170	71 ± 8	10.1 ± 0.9	3.4 ± 0.8	7.0 ± 1.0	3.7 ± 1.7

See also Figure S2 and Tables S2–S4.

partially explains their lack of inhibition of mutant switch-activated kinases that also predominantly populate the type I active conformation, such as exon 17 D816 mutant KIT (Table 1). Regorafenib, which is significantly more potent against fully phosphorylated KIT than imatinib and sunitinib, inhibits AL mutants that imatinib and sunitinib do not (see cellular data below). Nonetheless, regorafenib weakly inhibits exon 17 D816 KIT mutants. Thus, these exon 17 switch-activated mutants are resistant to all three FDA-approved type II tyrosine kinase inhibitor therapies for GIST. Strikingly, the type II inhibitors ripretinib, DP-5439, and DP-2976 inhibit both forms of WT KIT with <5-fold difference (half maximal inhibitory concentration [IC_{50}] range 2.7–15 nM) and are also potent against type I conformationally activated mutant kinases, including KIT exon 17 D816H and D816V (IC_{50} = 11–33 nM) (Table 1). The type I kinase inhibitors midostaurin and BLU-285 inhibit both forms of WT KIT as well as exon 17 D816 switch-activated mutants of KIT.

Ripretinib, DP-5439, and DP-2976 inhibit the activity of V654A KIT (IC_{50} = 11–28 nM), one of the most common imatinib-resistant mutants (Heinrich et al., 2006, 2008), as well as the gatekeeper mutant T670I (IC_{50} = 2.7–9.2 nM). Type I kinase inhibitors midostaurin (IC_{50} >3,000 nM) and BLU-285 (IC_{50} = 660 nM) are both weak inhibitors of V654A KIT in the presence of 1 mM ATP.

To confirm the above findings, ripretinib was also tested in *in vitro* binding assays with no ATP but in the presence of a competitive ligand (Table S2) (Fabian et al., 2005). Ripretinib tightly bound WT KIT (K_d = 7.8 nM) and PDGFRA (K_d = 21 nM), KIT exon 11 mutants V559D (K_d = 8.8 nM) and L576P (K_d = 24 nM), exon 11/13 double mutant V559D/V654A (K_d = 33 nM), exon 11/14 double mutant V559D/T670I (K_d = 25 nM), as well as exon 17 mutants D816H (K_d = 53 nM) and D816V (K_d = 13 nM), and an exon 18 AL mutant, A829P KIT (K_d = 11 nM). Ripretinib only weakly bound the autoinhibited form of WT KIT. DP-5439 had a similar profile to ripretinib (Table S2). Data for imatinib, sunitinib, and midostaurin in these binding assays have been published previously (Davis et al., 2011). In addition, ripretinib and DP-5439 were tested in a larger panel of KIT mutants in an assay using a low concentration of 10 μM ATP (Table S2). Both compounds had sub-nanomolar IC_{50} values for all exon 11 and exon 17 mutants tested, including D816V. Ripretinib also potently inhibited exon 13 mutants K642E (IC_{50} = 1.2 nM) and V654A (IC_{50} = 39 nM), as well as exon 14 mutant T670I (IC_{50} = 3.9 nM). DP-5439 had a similar profile (Table S2).

Ripretinib, DP-5439, and DP-2976 are also potent inhibitors of WT PDGFRA and the D842V mutant. BLU-285 is ~10-fold more potent than ripretinib as an inhibitor of D842V PDGFRA in an enzymatic assay at 1 mM ATP. Ripretinib is ~ 2-fold more potent than BLU-285 versus WT PDGFRA (Table 1). In summary, in enzymatic studies, ripretinib broadly inhibits all tested KIT and PDGFRA mutants, and has a superior composite profile to marketed and tested investigational agents (Table 1).

Ripretinib Kinase Profile

The kinome-wide profile of ripretinib, determined iteratively at 10 μM ATP then at approximate cellular levels of ATP (1–4 mM), is shown in Table S3. Kinase inhibitors must compete with high ATP levels in cells, therefore a large kinase panel run with low concentrations of ATP was followed by performing kinase assays at cellular levels of ATP and/or in cellular assays. This allows for a more complete representation of kinase inhibitor potency and selectivity at relevant cellular concentrations of ATP. Based on a composite (Figure S2B) of enzyme (Table S3) and cellular kinase phosphorylation data (Table S4), ripretinib inhibited four kinases with IC_{50} < 10 nM (DDR2, VEGFR2, PDGFRB, and TIE2), in addition to KIT and PDGFRA. Most of these kinases promote tumor growth and metastasis in the tumor microenvironment via angiogenesis, macrophage-mediated vasculogenesis, or immunomodulatory mechanisms (Coffelt et al., 2011; Folkman and Shing, 1992; Hanahan and Coussens, 2012; Joyce, 2005; Wyckoff et al., 2007). Ripretinib inhibited five additional kinases with an IC_{50} < 100 nM out of 300 kinases tested. Twenty-five other kinases were inhibited at higher concentrations (>100 nM IC_{50} < 1,000 nM), 15 of which exhibit IC_{50} values >100-fold higher than the IC_{50} value for KIT. The active metabolite DP-5439 exhibits a similar profile to the parent ripretinib (data not shown). Because *in vitro* kinase assay readouts are dependent on the conformation of the kinase construct, which can be artificial (e.g., truncated kinases or kinases with regulatory domains or complex protein interactions), inhibition of certain kinases was confirmed in cellular assays (Table S4).

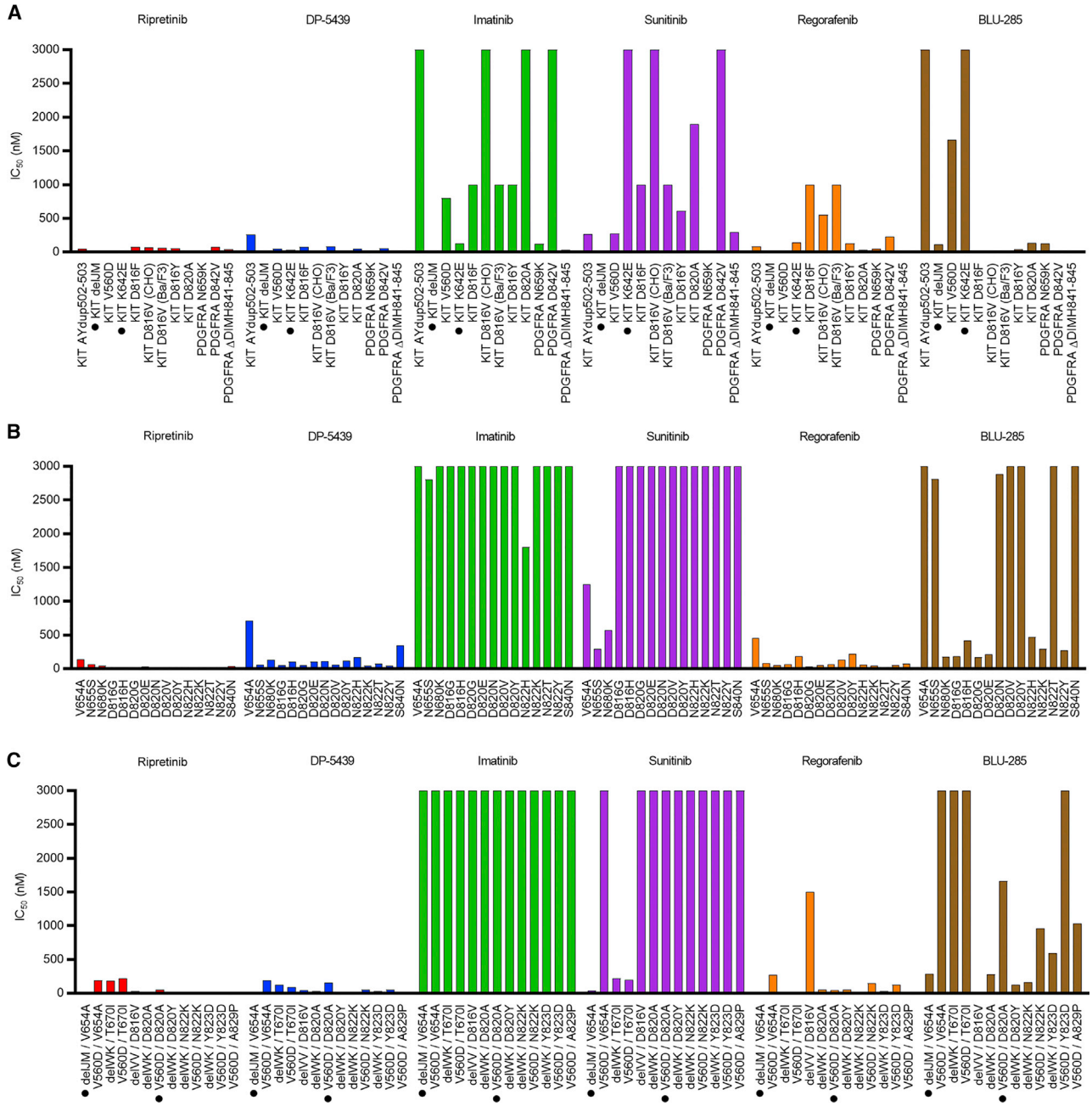

Figure 2. Inhibition of KIT and PDGFRA Mutants by Ripretinib, DP-5439, and Comparator Compounds in Cell-Based Assays

(A–C) IC_{50} values for inhibition of phosphorylation of KIT or PDGFRA in GIST or transfected CHO or Ba/F3 cells expressing primary KIT or PDGFRA mutations (A); CHO cells expressing KIT exon 9 primary mutations plus imatinib-resistant secondary mutations (B); GIST or transfected CHO cells expressing KIT exon 11 primary mutations plus imatinib-resistant secondary mutations (C). GIST cell lines are noted by dots. See also Figure S3.

Ripretinib was found to be more potent in cell assays than biochemical enzyme assays for VEGFR2, PDGFRB, and TIE2, likely due to the conformation and/or phosphorylation state of the native kinase in a cellular context. However, ripretinib was a weaker inhibitor of CSF1R in the cellular assay compared with the biochemical assay, as well as a much weaker inhibitor of BRAF and CRAF in cellular studies compared with biochemical studies (Table S4).

Ripretinib Broadly Inhibits a Large Panel of KIT and PDGFRA Mutants in GIST and Transfected Cell Lines

The activity of ripretinib against a broad range of KIT and PDGFRA mutants was evaluated in KIT mutant GIST cell lines (Bauer et al., 2006; Duensing et al., 2004), as well as in a large panel of CHO or Ba/F3 cells transfected with clinically identified primary and drug-resistant KIT or PDGFRA mutants (Figures 2A–2C). Inhibition of KIT or PDGFRA phosphorylation was assessed

Table 2. Inhibition of KIT Phosphorylation in GIST Cell Lines

	GIST T1 (ΔJMD) Exon 11	GIST 430 (ΔJMD/V654A) Exons 11/13	GIST 48 (V560D/D820A) Exons 11/17[a]	GIST 882 (K642E) Exon 13
	IC_{50} (nM)			
Ripretinib	3.0 ± 0.9	7.9 ± 2.1	53 ± 29	21 ± 10
DP-5439	7.3	15	150	30
Imatinib	12	>3,000	>3,000	122
Sunitinib	3	37	>3,000	>3,000
Regorafenib	2	9	41	137
BLU-285	110	285	1,660	>3,000

[a]GIST 48 cells are homozygous for V560D but heterozygous for the secondary resistance mutation D820A, and inhibition curves are biphasic. The IC_{50} value reflects the concentration needed to inhibit 50% phosphorylation of what is presumed to be the double mutant.

by ELISA or western blot. The most common primary mutations observed in GIST are found in exon 11 (~70%; resulting in disruption of the JMD inhibitory switch) or exon 9 (~10%; resulting in increased dimerization and activation). Kinase inhibitors are known to have differential effects on these two classes of primary mutations (Corless et al., 2011), and the effects of secondary mutations can be dependent on the context of the primary mutation (especially for certain mutations in exon 11 such as V560D and the exon 9 AY502-503 duplication) (Garner et al., 2014). A wide variety of the most commonly observed secondary resistance mutations were tested within the context of either exon 9 (Figure 2B) or exon 11 (Figure 2C) primary mutations. In addition, primary mutants of KIT observed in mastocytosis and AML, and primary mutants of PDGFRA in GIST were examined (Figure 2A).

Ripretinib and DP-5439 broadly inhibited mutant KIT phosphorylation in all GIST cell lines (Figure 2, noted with dots; Table 2; Figure S3) and transfected cell lines (Figure 2; Table 3), including highly treatment-resistant mutants such as D816V (ripretinib IC_{50} range across all mutants: 1.4–221 nM). Inhibition by imatinib, sunitinib, regorafenib, and BLU-285 are shown for comparison. Imatinib was potent versus the KIT exon 11 deletion mutant (delJM) GIST T1 cell line and in the KIT exon 13 mutant (K642E) GIST 882 cell line (Figure 2A), but was inactive in GIST 430 (exon 11 deletion/exon 13 V654A) and GIST 48 (exon 11 V560D/exon 17 D820A) cells as well as cells transfected with drug-resistant mutants, including AL mutations (Figure 2C). Sunitinib inhibited KIT exon 13 and exon 14 secondary mutants N655S, N680K, and T670I in the 37–570 nM range (Figures 2B and 2C). In this dataset, sunitinib inhibited V654A in the context of an exon 11 deletion (Figure 2C); however, it exhibited modest or no activity against V654A KIT transfected into CHO cells in the context of an exon 11 V560D (Figure 2C) or exon 9 AY502-503 duplication mutation (Figure 2B), possibly due to resistance versus these combinations of primary/secondary mutations or due to the transient overexpression which results in dimerization and full phosphorylation of the mutant kinases in these assays. Sunitinib has been shown to only inhibit unphosphorylated KIT mutants (Gajiwala et al., 2009). Sunitinib was inactive against all exon 17/18 AL mutants tested (IC_{50} > 1,000 nM; Figure 2; Table 3).

Ripretinib was effective in all imatinib- and sunitinib-resistant KIT mutants tested and was 3- to >50-fold more potent than regorafenib in 18 of 37 tested KIT mutants, with similar potency (~1- to 3-fold) observed in 17 out of 37 mutants. Ripretinib was weaker than regorafenib against only the T670I secondary KIT mutants (Figure 2C). Significantly, ripretinib was >2-fold more potent than regorafenib in 21 of 26 cell lines expressing KIT exon 17/18 switch-activating mutations, with similar potency in the other 5 cell lines. Importantly, ripretinib and metabolite DP-5439 are approximately 10- to 20-fold more potent than regorafenib versus the KIT D816V mutation (Figure 2A). BLU-285 lacked activity against the primary exon 9 AY502-503 duplication, as well as a V560D exon 11 primary mutation and the K642E exon 13 primary mutation (Figure 2A). BLU-285 exhibited weak inhibition of all KIT exon 13 and 14 secondary mutations tested in CHO cells except N680K in the context of an exon 9 primary mutation (Figure 2B) and in GIST 430 cells harboring a V654A mutation in the context of an exon 11 deletion primary mutation (Figure 2C) where it had moderate activity. Ripretinib was 7- to 450-fold more potent than BLU-285 against most (21 of 26 tested) AL exon 17/18 mutants (D816G/H, D820A/G/E/N/V/Y, N822H/K/T/Y, Y823D, A829P, and S840N), with the exception of five constructs incorporating D816F/V/Y where BLU-285 had 1.6- to 9-fold greater potency (Figure 2; Table 3). Interestingly, BLU-285 was much weaker against secondary mutations in the context of a V560D exon 11 primary mutation compared with an exon 11 deletion (Figure 2C) and also was inactive against many AL mutations in the context of an exon 9 primary mutation (Figure 2B).

BLU-285 was extremely potent against constructs incorporating D842V PDGFRA in transfected cells, in line with enzyme inhibition data above (Figure 2A; Table 3). Ripretinib and DP-5439 also inhibited D842V PDGFRA in CHO cells with IC_{50} values under 100 nM (Figure 2A; Table 3). Ripretinib potently blocked less common PDGFRA variants found in GIST (such as N659K and ΔDIMH841-845; IC_{50} = 7.8–39 nM). Ripretinib also potently blocked PDGFRA phosphorylation in PDGFRA-amplified H1703 lung cancer cells (IC_{50} = 6 nM; Table S4) and in Ba/F3 cells expressing PDGFRA exon 12 mutant V561D (IC_{50} = 25 nM; data not shown). In summary, in cellular studies, ripretinib comprehensively inhibits activating mutations across all six exons known to be mutated in KIT-driven GIST, and also inhibits mutations in PDGFRA in exons 12, 14, and 18.

Ripretinib Potently Blocks Proliferation in KIT and PDGFRA Mutant Cancer Cell Lines

Ripretinib and DP-5439 blocked proliferation of three GIST cell lines with equal or greater potency than imatinib,

Table 3. Inhibition of KIT or PDGFRA Phosphorylation in Transfected Cells

Mutation(s)	Exon(s)	Cell Line	Ripretinib IC_{50} (nM)	DP-5439	Imatinib	Sunitinib	Regorafenib	BLU-285
KIT AYdup502-503	9	CHO	44 ± 23	257	>3,000	262	83	>3,000
KIT AYdup502-503/V654A	9/13	CHO	140 ± 32	710	>3,000	1,250	455	>3,000
KIT AYdup502-503/N655S	9/13	CHO	63 ± 56	60	2,800	290	78	2,810
KIT AYdup502-503/N680K	9/14	CHO	47 ± 36	129	>3,000	570	53	173
KIT AYdup502-503/D816G	9/17	CHO	20 ± 10	48	>3,000	>3,000	66	182
KIT AYdup502-503/D816H	9/17	CHO	14 ± 6	102	>3,000	>3,000	180	416
KIT AYdup502-503/D820G	9/17	CHO	16 ± 5	54	>3,000	>3,000	28	165
KIT AYdup502-503/D820E	9/17	CHO	31 ± 5	99	>3,000	>3,000	53	215
KIT AYdup502-503/D820N	9/17	CHO	12 ± 2	111	>3,000	>3,000	68	2,880
KIT AYdup502-503/D820V	9/17	CHO	7.9 ± 1.5	57	>3,000	>3,000	129	>3,000
KIT AYdup502-503/D820Y	9/17	CHO	14 ± 9	116	>3,000	>3,000	216	>3,000
KIT AYdup502-503/N822H	9/17	CHO	25 ± 11	169	1,800	>3,000	57	467
KIT AYdup502-503/N822K	9/17	CHO	17 ± 9	47	>3,000	>3,000	44	291
KIT AYdup502-503/N822T	9/17	CHO	13 ± 3	72	>3,000	>3,000	15	>3,000
KIT AYdup502-503/N822Y	9/17	CHO	22 ± 8	44	>3,000	>3,000	50	272
KIT AYdup502-503/S840N	9/18	CHO	38 ± 23	343	>3,000	>3,000	74	>3,000
KIT ΔWKV557C/T670I	11/14	CHO	183 ± 104	121	>3,000	220	23	>3,000
KIT ΔV559-V560/D816V	11/17	CHO	26 ± 24	45	>3,000	>3,000	1,500	6.4
KIT ΔWKV557C/D820A	11/17	CHO	7.2 ± 4.0	26	>3,000	>3,000	50	279
KIT ΔWKV557C/D820Y	11/17	CHO	5.9 ± 3.0	21	>3,000	>3,000	51	127
KIT ΔWKV557C/N822K	11/17	CHO	1.4 ± 0.1	11	>3,000	>3,000	6.4	159
KIT ΔWKV557C/Y823D	11/17	CHO	5.3 ± 2.5	31	>3,000	>3,000	26	590
KIT V560D	11	CHO	4.0 ± 1.8	45	800	274	4.7	1,660
KIT V560D/V654A	11/13	CHO	189 ± 74	191	>3,000	>3,000	272	>3,000
KIT V560D/T670I	11/14	CHO	221 ± 90	88	>3,000	200	24	>3,000
KIT V560D/N822K	11/17	CHO	21 ± 5	49	>3,000	>3,000	145	956
KIT V560D/Y823D	11/17	CHO	23 ± 12	51	>3,000	>3,000	127	>3,000
KIT V560D/A829P	11/18	CHO	2.3 ± 1.2	18	>3,000	>3,000	15	1,030
KIT D816F	17	Ba/F3	75 ± 5	75	>1,000	>1,000	>1,000	14
KIT D816V	17	CHO	64 ± 25	21	>3,000	>3,000	550	7.4
KIT D816V	17	Ba/F3	57 ± 31	82	>1,000	>1,000	>1,000	14
KIT D816Y	17	Ba/F3	52 ± 20	19	>1,000	607	127	33
KIT D820A	17	CHO	6.7 ± 6.3	41	>3,000	1,900	26	131
PDGFRA N659K	14	Ba/F3	7.8 ± 7.9	14	120	14	42	125
PDGFRA D842V	18	CHO	72 ± 18	54	>3,000	>3,000	223	0.10
PDGFRA ΔDIMH841-845	18	Ba/F3	39 ± 16	9	29	290	17	4

sunitinib, regorafenib, midostaurin, and BLU-285, with the exception of the T670I-resistant mutant GIST T1 5R cell line, where sunitinib and regorafenib had greater potency (Table 4). In mastocytosis, >90% of patients have a KIT D816V mutation and ~5% of AML patients have an exon 17 mutation in KIT kinase. The mouse mastocytoma cell line P815 has a KIT D814Y mutation (equivalent to D816Y in human KIT). The human mast cell line HMC1.1 has a primary exon 11 V560G KIT mutation (Sundstrom et al., 2003). A drug-resistant version of this cell line, HMC1.2, has a KIT D816V mutation in addition to V560G, more closely mimicking KIT D816V mutant mast cells in mastocytosis patients. The Kasumi-1 human AML cell line has a primary exon 17 N822K mutation in KIT. Ripretinib and DP-5439 potently block proliferation of these mast cell and AML cell lines (Table 4) with a superior profile compared with other compounds. Of note, the D816V mutation is heterozygous in HMC1.2 cells, but the exon 11 mutation is homozygous, thus mutant KIT expressed from both alleles may need to be inhibited to block proliferation. BLU-285 has greater potency for exon 17 D816V than exon 11 mutations (Tables 2, 3, and 4), thus its inhibition of HMC1.2 proliferation is likely related to the composite inhibition of both expressed alleles. BLU-285 is a potent inhibitor of the proliferation of Ba/F3 cells expressing D816V KIT (Table 4). Ripretinib and DP-5439 also potently inhibit proliferation of Ba/F3 D816V KIT cells.

Table 4. Inhibition of Cell Proliferation in KIT and PDGFRA Mutant Cell Lines

	GIST T1 (ΔJMD) KIT Exon 11	GIST T1 5R (ΔJMD/T670I) KIT Exons 11/14	GIST T1 Juke (ΔJMD/D816E) KIT Exons 11/17	P815 (D814Y) KIT Exon 17	Kasumi-1 (N822K) KIT Exon 17	HMC1.1 (V560G) KIT Exon 11	HMC1.2 (V560G/ D816V) KIT Exons 11/17	Ba/F3 (D816V) KIT Exon 17	Ba/F3 (D842V) PDGFRA Exon 18
	IC_{50} (nM)								
Ripretinib	3.2 ± 1.5	134 ± 30	23 ± 17	23 ± 10	3.4 ± 1.5	1.9 ± 0.7	47 ± 28	10.2 ± 8.2	56 ± 22
DP-5439	2.6 ± 1.1	141 ± 24	14 ± 1	41 ± 9	2.5 ± 0.9	1.9 ± 0.3	47 ± 23	17 ± 12	138 ± 65
Imatinib	9.2 ± 4.0	>3,000	127 ± 11	>3,000	270 ± 180	10.7 ± 1.4	>3,000	>3,000	841 ± 444
Sunitinib	2.8 ± 1.1	8.8 ± 0.7	397 ± 79	174 ± 79	33 ± 26	1.3 ± 0.6	1,410 ± 770	417 ± 196	349 ± 88
Regorafenib	46 ± 5	42 ± 6	183 ± 35	>3,000	48 ± 4	11.9 ± 3.8	>3,000	1,750 ± 690	341 ± 28
Midostaurin	124 ± 23	101 ± 5	283 ± 21	151 ± 24	37 ± 21	473 ± 245	270 ± 210	34 ± 9	104 ± 16
BLU-285	41 ± 19	175 ± 17	75 ± 41	22 ± 8	15 ± 6	120 ± 31	147 ± 57	2.1 ± 0.6	3.2 ± 0.9

Ripretinib and DP-5439 also blocked proliferation of cells driven by PDGFRA variants. Both compounds inhibited the growth of Ba/F3 cells expressing D842V PDGFRA (Table 4). Ripretinib also blocked cell proliferation (IC_{50} = 9 nM) of *PDGFRA*-amplified H1703 lung cancer cells as well as FIP1L1-PDGFRA fusion EOL1 hypereosinophilic leukemia cells (IC_{50} < 1 nM), and DP-5439 had similar activity in these PDGFRA-driven cell lines (data not shown). In summary, ripretinib broadly inhibits proliferation of cell lines driven by alterations in KIT or PDGFRA, relevant in GIST, SM, leukemia, and lung cancer.

Ripretinib Prevents the Outgrowth of Resistant KIT Mutant Clones in Saturation Mutagenesis Assays

Ba/F3 cells were stably transfected with V560D KIT kinase and proliferated independently of interleukin-3 (IL-3) supplementation. To perform saturation mutagenesis, cells were treated with the mutagen ethylnitrosourea (ENU), washed several times, and then plated in wells containing ripretinib or imatinib. Cells that grew in the presence of inhibitor were expanded, and the KIT gene (exons 8–21) was sequenced to identify possible resistance mutations.

No secondary mutations were identified in cells treated with ripretinib, even at the low concentration of 25 nM. Resistant mutations in KIT were identified in cells treated with imatinib at all three concentrations tested (100, 250, and 500 nM), including the gatekeeper mutation T670I and AL switch mutation D816V, both well-known imatinib-resistant mutations, as well as K807E, another known, but rarer site of resistance. A small percentage of wells had cell growth in the presence of imatinib or ripretinib, in which no secondary mutation in KIT was identified. Due to the random mutagenesis that occurs after ENU treatment, these cells may have gained activating mutations in other kinases or pathways and become independent of the requirement of KIT activity. Ba/F3 cells are known to be able to grow independently of IL-3 with a variety of different activated kinases (Melnick et al., 2006).

Saturation mutagenesis was also performed starting with the primary AL mutant D816V, mimicking treatment of aggressive SM to determine what resistance mutations might be observed. Ripretinib potently inhibits the KIT D816V mutation (Tables 1 and 3). To perform saturation mutagenesis, Ba/F3 mutant KIT D816V cells were treated with ENU, washed several times, and then allowed to recover for 7 days, before adding DCC-2618 to the plates. At 500 nM ripretinib, no drug-resistant clones were identified, indicating that ripretinib can prevent mutational escape even when starting from an AL mutant that is highly shifted toward the active conformation.

Ripretinib Blocks KIT Phosphorylation and Tumor Growth *In Vivo*

Ripretinib exhibited inhibition of KIT phosphorylation in an exon 11 deletion mutant KIT GIST T1 cell line xenograft for up to 12 h following single oral dosing (Figures S4A and S4B). Pharmacokinetic/pharmacodynamic (PK/PD) dose response (Figure S4A, 2 h time point) data demonstrate that low plasma concentrations are sufficient for KIT inhibition (51% inhibition at 227 ng/mL; 84% inhibition at 740 ng/mL). In time course PK/PD studies, KIT signaling was suppressed by 69%–88% at 8 h after administration of a single oral dose of 50 mg/kg ripretinib and by ~40% at 12 h post-dose (Figure S4B). Ripretinib has an active metabolite, DP-5439, in preclinical species and humans, which achieves exposure (area under the curve [AUC]) roughly equivalent to the exposure of the parent drug in mice (data not shown). The 24-h combined AUC of both ripretinib and metabolite DP-5439 after a 50 mg/kg oral dose of ripretinib was ~5,000 ng*h/mL.

Before the initiation of efficacy studies, the maximum tolerated dose (MTD) of ripretinib in mice was determined. Ripretinib was administered orally for 14 days with doses ranging from 30 mg/kg twice daily (BID) to 180 mg/kg BID. The MTD was determined to be >180 mg/kg BID, with ripretinib reaching 2,290 ng/mL at 2 h after the final dose. Treatment at all doses produced neither treatment-related mortality nor body weight loss (Figure S4C). Necropsies at study termination revealed no remarkable findings. The no observed adverse effect level (NOAEL) in a 4-week pivotal rat toxicology study was 300 mg/kg/day, corresponding to a combined C_{max} and 24-h AUC of ripretinib and metabolite DP-5439 of ~4,000 ng/mL and 32,000 ng*h/mL in female rats, respectively (Table S5). The NOAEL AUC affords a therapeutic index of ~3.2 above observed efficacious exposures in mice (at 100 mg/kg/day doses).

Based on this safety profile, ripretinib was formulated into a mouse diet to achieve approximate levels of 100 and 25 mg/kg/day in mouse efficacy studies. In the GIST T1 model

treated with ripretinib, significant tumor regression was observed at both doses (Figure 3A). At the high dose, 6/10 mice had complete tumor regression, with the remaining 4/10 mice having partial tumor regression during the dosing period. At the low dose, 2/10 mice had complete tumor regression, and 6/10 had partial tumor regression. Tumors exhibited slow regrowth after the end of the dosing period. Survival to study endpoint (day 68) was 100% for ripretinib-treated mice and 25% for vehicle-treated mice (Figure 3B). Body weight changes for ripretinib-treated groups were similar to vehicle (Figure S4D).

Ripretinib was next evaluated in an imatinib-resistant GIST patient-derived xenograft (PDX) model, which expressed mutant KIT containing a primary JMD deletion of residues W557 and K558, as well as a secondary exon 17 AL Y823D mutation (Figure 3C). Upon repeated dosing at 100 mg/kg once daily (QD) or 50 mg/kg BID ripretinib, tumor growth was blocked while on drug (through day 28), with tumors exhibiting regression with the BID dosing regimen. Twice daily dosing was likely superior to once daily dosing in this model due to inhibition of KIT for the entire 24-h period each day, as single daily doses are largely cleared by 12 h in mice (Figure S4B). Survival to study endpoint (day 57) was 100% and 90% for 50 mg/kg BID and 100 mg/kg QD ripretinib-treated mice, respectively, and 10% for vehicle-treated mice (Figure 3D). KIT signaling was inhibited in this model, with phosphorylation of KIT as well as downstream phosphorylation of AKT, ERK, and STAT5 reduced at both doses (Figure 3E). Body weight changes for ripretinib-treated groups were similar to vehicle (Figure S4E).

Ripretinib blocked tumor growth in a P815 murine mastocytoma allograft model (KIT D814Y) when dosed in the diet at 100 mg/kg/day (Figure 3F). Ripretinib also was efficacious in the HMC1.2 mast cell xenograft model (KIT V560G/D816V) (Figure 3G). In the H1703 PDGFRA-amplified lung cancer xenograft model (Figure 3H), ripretinib led to complete or partial tumor regression in 8/10 and 2/10 mice, respectively, at 100 mg/kg/day, with tumors slowly regrowing after cessation of treatment. One week after ending treatment with ripretinib, 4/10 mice had complete tumor regression and 3/10 had partial regression. At the lower dose of 25 mg/kg/day ripretinib, treatment led to 90% inhibition of tumor growth during the dosing period.

Ripretinib Demonstrates Preliminary Clinical Benefit in Patients with Heterogeneous Drug-Resistant KIT Mutants in a Phase 1 Clinical Trial

Based on the compelling preclinical data indicating that ripretinib can broadly inhibit primary and secondary mutations in KIT, the safety and tolerability of ripretinib was tested in a First-in-Human study (NCT02571036). Ripretinib was administered orally, once or twice daily in cycles of 28 days, and radiographic response was assessed per Response Evaluation Criteria in Solid Tumors (RECIST1.1). Preliminary data suggest that ripretinib leads to durable disease control in drug-resistant metastatic GIST patients with a broad spectrum of KIT mutations. Two patients enrolled during the dose escalation phase of the study are described. Patient 1 was a 62-year-old male fourth-line GIST patient who progressed on all approved treatment options (i.e., imatinib, sunitinib, and regorafenib) before enrollment in the study. The patient was enrolled in the 50 mg BID dose escalation cohort and had substantial tumor burden due to multiple liver and non-target bony metastases. Plasma cell-free DNA (cfDNA) analysis at baseline demonstrated significant mutant allele frequency (MAF) of a primary exon 11 KIT deletion (V559_G565del) and secondary (i.e., drug-resistant) KIT mutations in exon 13 (V654A) and exon 18 (A829P; Figure 4A). Patient 1 had steady-state (cycle 1 day 15) PK parameters for ripretinib + metabolite DP-5439 of C_{max} = 1,820 ng/mL (or ~3.6 μM) and C_{min} = 1,120 ng/mL (~2.2 μM) (Figure S4F). At C_{max} (and C_{min}) these values are ~19-fold (~12-fold) and >200-fold (>120-fold) above the IC_{50} values for ripretinib and DP-5439 against an exon 11 primary with a secondary V654A mutant or A829P secondary mutant, respectively (see Table 3). Patient 2 was a 56-year-old female fourth-line GIST patient who progressed on all approved tyrosine kinase inhibitors (TKIs) (i.e., imatinib, sunitinib, and regorafenib). The patient had significant MAF of a primary exon 11 deletion/insertion (Y568_L576delinsCV) and two drug-resistant exon 17 KIT mutations (D816E and D820Y) detected in cfDNA at baseline and was assigned to the 150-mg BID dose escalation cohort (Figure 4B). Patient 2 had steady-state (cycle 1 day 15) PK parameters for ripretinib + metabolite DP-5439 of C_{max} = 7,880 ng/mL (or ~15.8 μM) and C_{min} = 6,550 ng/mL (~13.1 μM) (Figure S4). At C_{max} (and C_{min}) these values are >350-fold (>290-fold) and >750-fold (>625-fold) above the IC_{50} values for ripretinib and DP-5439 against an exon 11 primary with a secondary D816 mutant or D820Y secondary mutant, respectively (Table 3).

At the first assessment, both patients experienced a dramatic and sustained reduction of circulating tumor DNA (ctDNA) MAF (patient 1 after 2 and patient 2 after 6 cycles) and, as of August 10, 2018, remained on treatment for 26 and 21 months, respectively, with best response in both patients of stable disease.

DISCUSSION

Ripretinib was designed to be a potent inhibitor of the full spectrum of primary and secondary drug-resistant mutants of KIT and PDGFRA. Ripretinib is a type II kinase inhibitor that shows strong activity against all tested exon 17/18 mutations in KIT and exon 18 mutations in PDGFRA. These mutations are located in the kinase ALs and predispose KIT or PDGFRA to active type I conformations. Even though it is a type II inhibitor, ripretinib (and metabolite DP-5439) exhibit cellular potency for inhibition of these AL mutants that is comparable with or superior to the type I inhibitors midostaurin or BLU-285. A co-crystal structure of a closely related analog of ripretinib (DP-2976) was solved, which demonstrates key elements of switch control inhibition. Certain elements of the inhibitor structure antagonize AL switch occupancy of the KIT type I active conformation, and other elements of the inhibitor stabilize the AL switch in the type II inactive conformation. In addition, inhibitor occupancy of the inhibitory vertical R-spine provides a surrogate for the loss-of-function mutation frequently observed in the exon 11 JMD inhibitory switch. These interactions in composite translate to potent and durable inhibition of KIT and broad-based inhibition of KIT activating mutations.

Ripretinib inhibits mutant KIT and PDGFRA activity in enzyme assays at physiologic levels of ATP, including mutants resistant to imatinib, sunitinib, and regorafenib. In general, data from

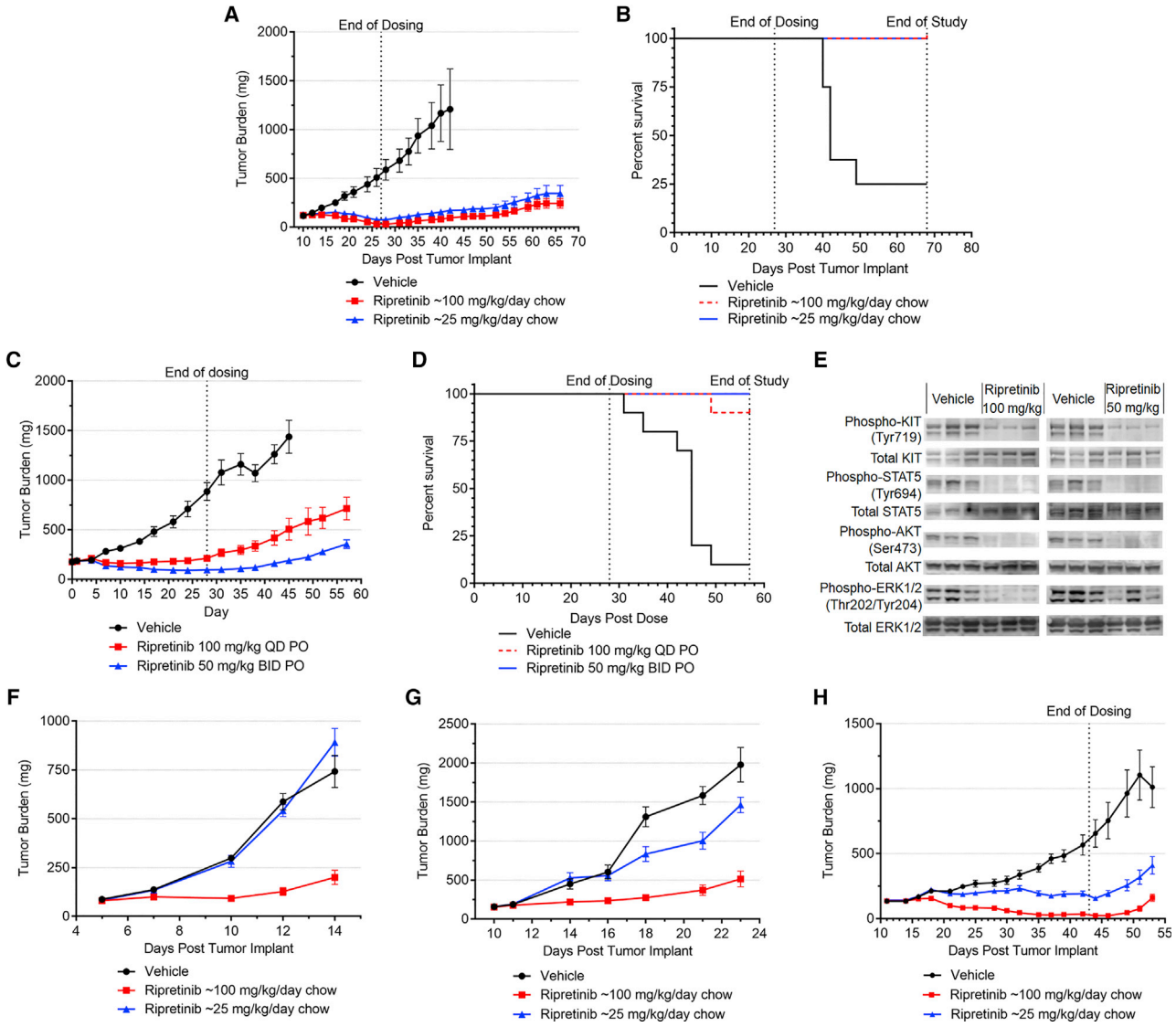

Figure 3. Inhibition of Tumor Growth by Ripretinib in GIST, Mastocytosis, and Lung Cancer Xenograft Models

(A) GIST T1 xenograft tumor growth in mice treated with ripretinib formulated into the mouse diet to achieve approximately 100 mg/kg/day (red) or 25 mg/kg/day (blue). Mice (n = 8–10 per cohort) were treated with ripretinib-formulated diet from day 10 to day 27. Data are represented as mean ± SEM.

(B) Survival to study endpoint in the GIST T1 xenograft model. Mice (n = 8–10 per cohort) were treated with ripretinib-formulated diet from day 10 to day 27.

(C) GIST PDX with a KIT exon 11 deletion and exon 17 Y823D mutation treated with ripretinib dosed orally at 100 mg/kg QD (red) or 50 mg/kg BID (blue). Mice (n = 10 per cohort) were dosed on day 0 through day 28. Data are represented as mean ± SEM.

(D) Survival to study endpoint in the GIST PDX model. Mice (n = 10 per cohort) were dosed on day 0 through day 28.

(E) KIT autophosphorylation and downstream phosphorylation of STAT5, AKT, and ERK1/2 in GIST PDX (exon 11 deletion/exon 17 Y823D) tumors 2 h after the final dose after 5 days of dosing ripretinib at 100 mg/kg QD or 50 mg/kg BID.

(F) Tumor growth in exon 17 D814Y mutant KIT P815 murine mastocytoma xenograft treated with ripretinib formulated into the mouse diet to achieve approximately 100 mg/kg/day (red) or 25 mg/kg/day (blue). Mice (n = 10 per cohort) were treated with ripretinib-formulated diet from day 5 to day 14. Data are represented as mean ± SEM.

(G) Tumor growth in exon 11/17 V560G/D816V mutant KIT HMC1.2 mast cell xenograft treated with ripretinib formulated into the mouse diet to achieve approximately 100 mg/kg/day (red) or 25 mg/kg/day (blue). Mice (n = 10 per cohort) were treated with ripretinib-formulated diet from day 10 to day 23. Data are represented as mean ± SEM.

(H) Inhibition of tumor growth in the *PDGFRA*-amplified H1703 lung cancer xenograft model treated with ripretinib formulated into the mouse diet to achieve approximately 100 mg/kg/day (red) or 25 mg/kg/day (blue). Mice (n = 10 per cohort) were treated with ripretinib-formulated diet from day 11 to day 43. Data are represented as mean ± SEM.

See also Figure S4.

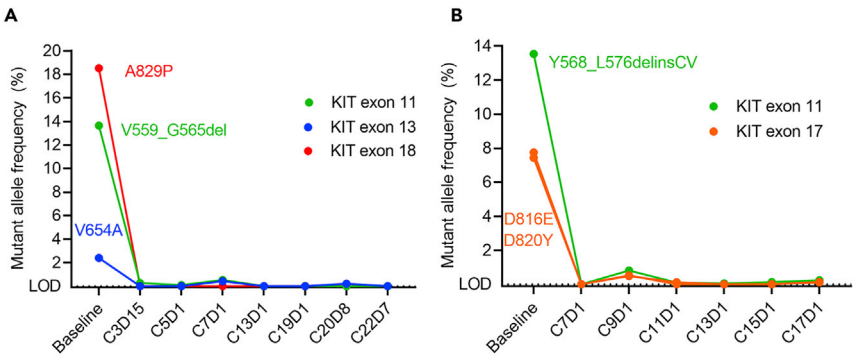

Figure 4. Durable Clinical Benefit and Pharmacodynamic Inhibition of Heterogeneous Drug-Resistant KIT Mutants in GIST Patients by Ripretinib

(A) In a fourth-line GIST patient assigned to the escalation cohort of 50 mg BID ripretinib, the pharmacodynamics of mutant allele frequency of the 1^{ry} KIT exon 11 mutation and 2^{ry} exon 13 and 18 mutations was detected in plasma cell-free DNA (the dashed line marks the lower limit of detection (LOD) of the assay, a MAF of 0.01%).

(B) In a fourth-line GIST patient receiving 150 mg BID ripretinib, the pharmacodynamics of mutant allele frequency of KIT exon 11 mutation and 17 mutations was detected in plasma cell-free DNA. See also Table S5.

kinase assays run at low ATP are often quite divergent from cellular inhibition, since most kinase inhibitors compete with ATP for binding to the kinase. In addition, mutant kinases, including KIT and PDGFRA mutants, have significantly lower $K_{M,\ ATP}$ values than WT, thus testing at low ATP can lead to disparate results compared with testing activity in whole cells. Ripretinib was tested at mM levels of ATP in kinase assays or in cellular assays where possible. Ripretinib is potent against KIT and PDGFRA mutants in a broad range of cell-based assays and outperforms competitor type I or type II compounds. Table 1 summarizes the KIT and PDGFRA profile of ripretinib alongside imatinib, sunitinib, regorafenib, and the investigational agent BLU-285. The KIT and PDGFRA profile of BLU-285 was recently published (Evans et al., 2017). The potencies in this paper were obtained at ATP concentrations at $K_{M,\ ATP}$ values for each of the kinases (1–100 μM ATP). We determined the potency of BLU-285 at a cellular level of ATP concentration (1 mM). These differences in experimental methods likely explain the differences reported here versus those previously published. Notably, in cellular assays, ripretinib exhibits potency versus KIT exon 9 AY502-503 duplication primary mutation alone or coupled with various exon 13, 14, and 17 secondary mutations, a profile superior to that of imatinib, sunitinib, and BLU-285. Ripretinib also potently inhibits KIT exon 13 V654A as a primary mutation or as a secondary resistance mutation. V654A is the most widely reported KIT resistance mutation to imatinib, thus the ability to inhibit V654A in GIST patients is important. In addition, despite being a type II inhibitor, ripretinib exhibits the broadest profile for inhibition of a panel of exon 17 KIT AL mutations compared with all other tested agents. Ripretinib blocks proliferation of cell lines harboring KIT exon 17 mutations, exhibiting potency superior to all other agents across the spectrum of KIT exon 17 mutant cell lines.

In most patients with GIST, a *KIT* exon 9 or exon 11 mutation is the primary driver mutation of the cancer. However, after treatment with imatinib, sunitinib, and/or regorafenib, secondary drug resistance mutations can be found in *KIT* exons 13, 14, 17, and 18. Furthermore, since most patients undergoing treatment with TKIs have metastatic GIST, different tumor sites may have multiple distinct resistant mutations (Liegl et al., 2008). A drug that inhibits one or only a subset of these mutations is less likely to be successful due to some metastatic sites continuing to grow even if other sites are effectively treated. Thus, an agent capable of inhibition of the broadest spectrum of KIT mutations is necessary for global disease control in GIST. Ripretinib broadly inhibits all known clinically relevant KIT and PDGFRA mutants.

Furthermore, no resistant clones were identified in saturation mutagenesis studies with ripretinib starting with an exon 11 KIT mutant (V560D) or an exon 17 (D816V) KIT mutant. The lack of resistant cell outgrowth in the Ba/F3 KIT D816V saturation mutagenesis study is significant, as secondary resistance mutations in exons 9, 11, and 13, including AY502-503dup, V560D, or K642E have been reported in mastocytosis patients (Lasho et al., 2016). Ripretinib could serve as a potentially effective single-agent treatment in earlier stage patients to prevent the emergence of resistance.

Ripretinib exhibits efficacy in xenograft models including GIST T1, an exon 17 drug-resistant GIST PDX model, two models of SM, and a *PDGFRA*-amplified lung cancer model. In GIST T1, imatinib-resistant GIST PDX, and H1703 lung cancer models, dosing with ripretinib led to tumor regressions.

Ripretinib was evaluated in a phase 1 clinical trial for the treatment of advanced malignancies with a focus on GIST. Significant plasma cfDNA MAF reduction across all KIT exons has been presented previously for ripretinib (George et al., 2018). Herein, the dramatic reduction of heterogeneous resistant KIT mutations in patients is described, encompassing KIT exons 11, 13, 17, and 18 in two patients with long-term disease control on ripretinib. These observed pharmacodynamic (PD) effects included the V654A mutation, where reduction below the level of detection was observed the first time in patient 1 at 50 mg BID, and provided evidence that concentrations observed *in vitro* can be achieved in humans. This finding supported the notion that dose levels equal or above 100 mg/day are active even against less-sensitive mutations and supported the dose selection of 150 mg QD as the recommended phase 2 dose. In addition to the compelling PD activity, objective tumor responses and durable clinical benefit have been reported in patients who progressed on between one to six prior lines of treatment (George et al., 2018; Janku et al., 2017). Thus, ripretinib may be able to address known liabilities in mutant coverage of clinical KIT inhibitors and is currently being studied in two phase 3 trials: INVICTUS, a randomized placebo-controlled trial in fourth-line and fourth-line plus GIST patients (NCT03353753), and

INTRIGUE, a randomized second line GIST trial evaluating ripretinib versus sunitinib (NCT03673501).

STAR★METHODS

Detailed methods are provided in the online version of this paper and include the following:

- KEY RESOURCES TABLE
- CONTACT FOR REAGENT AND RESOURCE SHARING
- EXPERIMENTAL MODEL AND SUBJECT DETAILS
  - Human Subjects
  - Mouse Models
  - Cell Lines and Culture Conditions
  - Insect Cells
- METHOD DETAILS
  - Chemical Synthesis
  - Protein Production for Crystallograpy
  - X-Ray Crystallography
  - Kinase Assays
  - Cell Proliferation Assays
  - Enzyme-Linked Immunosorbent assays
  - Western Blot Assays
  - Saturation Mutagenesis
  - Mouse Xenograft Models
  - Ripretinib Phase 1 Study
- QUANTIFICATION AND STATISTICAL ANALYSIS
- DATA AND SOFTWARE AVAILABILITY
- ADDITIONAL RESOURCES

SUPPLEMENTAL INFORMATION

Supplemental Information can be found online at https://doi.org/10.1016/j.ccell.2019.04.006.

ACKNOWLEDGMENTS

The authors thank J. Fletcher for GIST 48, GIST 430, and GIST 882 cell lines, B. Rubin for GIST T1 5R (T670I) and GIST T1 Juke (D816E), and T. Taguchi for GIST T1 KIT mutant cells. B.D.S. would like to dedicate this paper to Prof. Ronald T. Raines on the occasion of his 60th birthday.

AUTHOR CONTRIBUTIONS

Conceptualization, D.L.F., B.D.S., M.D.K., and S.C.W.; Experimental Design, B.D.S., S.C.W., A.G., W.-P.L., S.L.B., T.J.R., M.C.H., and D.L.F.; Experimental Work and Data Interpretation, B.D.S., A.G., W.-P.L., T.J.R., G.A.-A., S.L.B., L.C., M.M.H., C.B.L., D.F.M., B.A.T., and S.V.; Chemistry, M.D.K., Y.M.A., T.M.C., C.L.E., W.C.P., H.T., L.V., T.Y., and K.Y.; Clinical Study Design and Analysis, F.J., Y.S., R.R.-S., and O.R.; Patient Treatment, F.J. and A.R.A.R.; Writing, B.D.S., O.R., M.C.H., and D.L.F.

DECLARATION OF INTERESTS

B.D.S., M.D.K., W.P.L., A.G., C.B.L., Y.M.A., G.A.A., S.L.B., T.M.C., R.R.S., Y.S., H.T., L.V., S.V., K.Y., and D.L.F. are employees and shareholders of Deciphera Pharmaceuticals. O.R. is an employee of Deciphera Pharmaceuticals. D.L.F. is founder of Deciphera Pharmaceuticals and a member of its scientific advisory board. S.C.W., T.J.R., C.L.E., M.M.H., W.C.P., and B.A.T. are former employees of Deciphera Pharmaceuticals. L.C. is a former employee of Emerald Biostructures, which was a paid CRO of Deciphera Pharmaceuticals. A.M., A.T., and M.C.H. received financial support from Deciphera Pharmaceuticals for conduct of preclinical studies. F.J., A.R.A.R., and M.C.H. are principal investigators on the clinical study of ripretinib. F.J. and M.C.H. are on the Deciphera Clinical Advisory Board. M.C.H. has equity interest in MolecularMD, consults with MolecularMD, has provided expert testimony for Novartis, and consults with Blueprint Medicines. Deciphera Pharmaceuticals has patents on ripretinib and on its method of use.

Received: November 9, 2018
Revised: February 18, 2019
Accepted: April 15, 2019
Published: May 13, 2019

REFERENCES

Ahn, Y.M., Clare, M., Ensinger, C.L., Hood, M.M., Lord, J.W., Lu, W.P., Miller, D.F., Patt, W.C., Smith, B.D., Vogeti, L., et al. (2010). Switch control pocket inhibitors of p38-MAP kinase. Durable type II inhibitors that do not require binding into the canonical ATP hinge region. Bioorg. Med. Chem. Lett. *20*, 5793–5798.

Anastassiadis, T., Deacon, S.W., Devarajan, K., Ma, H., and Peterson, J.R. (2011). Comprehensive assay of kinase catalytic activity reveals features of kinase inhibitor selectivity. Nat. Biotechnol. *29*, 1039–1045.

Arock, M., Sotlar, K., Akin, C., Broesby-Olsen, S., Hoermann, G., Escribano, L., Kristensen, T.K., Kluin-Nelemans, H.C., Hermine, O., Dubreuil, P., et al. (2015). KIT mutation analysis in mast cell neoplasms: recommendations of the European Competence Network on Mastocytosis. Leukemia *29*, 1223–1232.

Bauer, S., Yu, L.K., Demetri, G.D., and Fletcher, J.A. (2006). Heat shock protein 90 inhibition in imatinib-resistant gastrointestinal stromal tumor. Cancer Res. *66*, 9153–9161.

Beadling, C., Jacobson-Dunlop, E., Hodi, F.S., Le, C., Warrick, A., Patterson, J., Town, A., Harlow, A., Cruz, F., 3rd, Azar, S., et al. (2008). KIT gene mutations and copy number in melanoma subtypes. Clin. Cancer Res. *14*, 6821–6828.

Bibi, S., Langenfeld, F., Jeanningros, S., Brenet, F., Soucie, E., Hermine, O., Damaj, G., Dubreuil, P., and Arock, M. (2014). Molecular defects in mastocytosis: KIT and beyond KIT. Immunol. Allergy Clin. North Am. *34*, 239–262.

Blay, J.Y. (2011). A decade of tyrosine kinase inhibitor therapy: historical and current perspectives on targeted therapy for GIST. Cancer Treat. Rev. *37*, 373–384.

Blume-Jensen, P., and Hunter, T. (2001). Oncogenic kinase signalling. Nature *411*, 355–365.

Brennan, C.W., Verhaak, R.G., McKenna, A., Campos, B., Noushmehr, H., Salama, S.R., Zheng, S., Chakravarty, D., Sanborn, J.Z., Berman, S.H., et al. (2013). The somatic genomic landscape of glioblastoma. Cell *155*, 462–477.

Chan, W.W., Wise, S.C., Kaufman, M.D., Ahn, Y.M., Ensinger, C.L., Haack, T., Hood, M.M., Jones, J., Lord, J.W., Lu, W.P., et al. (2011). Conformational control inhibition of the BCR-ABL1 tyrosine kinase, including the gatekeeper T315I mutant, by the switch-control inhibitor DCC-2036. Cancer Cell *19*, 556–568.

Coffelt, S.B., Chen, Y.Y., Muthana, M., Welford, A.F., Tal, A.O., Scholz, A., Plate, K.H., Reiss, Y., Murdoch, C., De Palma, M., and Lewis, C.E. (2011). Angiopoietin 2 stimulates TIE2-expressing monocytes to suppress T cell activation and to promote regulatory T cell expansion. J. Immunol. *186*, 4183–4190.

Cools, J., DeAngelo, D.J., Gotlib, J., Stover, E.H., Legare, R.D., Cortes, J., Kutok, J., Clark, J., Galinsky, I., Griffin, J.D., et al. (2003). A tyrosine kinase created by fusion of the PDGFRA and FIP1L1 genes as a therapeutic target of imatinib in idiopathic hypereosinophilic syndrome. N. Engl. J. Med. *348*, 1201–1214.

Corless, C.L., Barnett, C.M., and Heinrich, M.C. (2011). Gastrointestinal stromal tumours: origin and molecular oncology. Nat. Rev. Cancer *11*, 865–878.

Davis, M.I., Hunt, J.P., Herrgard, S., Ciceri, P., Wodicka, L.M., Pallares, G., Hocker, M., Treiber, D.K., and Zarrinkar, P.P. (2011). Comprehensive analysis of kinase inhibitor selectivity. Nat. Biotechnol. *29*, 1046–1051.

Demetri, G.D., Reichardt, P., Kang, Y.K., Blay, J.Y., Rutkowski, P., Gelderblom, H., Hohenberger, P., Leahy, M., von Mehren, M., Joensuu, H., et al. (2013). Efficacy and safety of regorafenib for advanced gastrointestinal stromal tumours after failure of imatinib and sunitinib (GRID): an international,

multicentre, randomised, placebo-controlled, phase 3 trial. Lancet *381*, 295–302.

Demetri, G.D., van Oosterom, A.T., Garrett, C.R., Blackstein, M.E., Shah, M.H., Verweij, J., McArthur, G., Judson, I.R., Heinrich, M.C., Morgan, J.A., et al. (2006). Efficacy and safety of sunitinib in patients with advanced gastrointestinal stromal tumour after failure of imatinib: a randomised controlled trial. Lancet *368*, 1329–1338.

DiNitto, J.P., Deshmukh, G.D., Zhang, Y., Jacques, S.L., Coli, R., Worrall, J.W., Diehl, W., English, J.M., and Wu, J.C. (2010). Function of activation loop tyrosine phosphorylation in the mechanism of c-Kit auto-activation and its implication in sunitinib resistance. J. Biochem. *147*, 601–609.

Duensing, A., Medeiros, F., McConarty, B., Joseph, N.E., Panigrahy, D., Singer, S., Fletcher, C.D., Demetri, G.D., and Fletcher, J.A. (2004). Mechanisms of oncogenic KIT signal transduction in primary gastrointestinal stromal tumors (GISTs). Oncogene *23*, 3999–4006.

Emsley, P., Lohkamp, B., Scott, W.G., and Cowtan, K. (2010). Features and development of Coot. Acta Crystallogr D. Biol. Crystallogr *66*, 486–501.

Evans, E.K., Gardino, A.K., Kim, J.L., Hodous, B.L., Shutes, A., Davis, A., Zhu, X.J., Schmidt-Kittler, O., Wilson, D., Wilson, K., et al. (2017). A precision therapy against cancers driven by KIT/PDGFRA mutations. Sci. Transl. Med. *9*, https://doi.org/10.1126/scitranslmed.aao1690.

Fabian, M.A., Biggs, W.H., 3rd, Treiber, D.K., Atteridge, C.E., Azimioara, M.D., Benedetti, M.G., Carter, T.A., Ciceri, P., Edeen, P.T., Floyd, M., et al. (2005). A small molecule-kinase interaction map for clinical kinase inhibitors. Nat. Biotechnol. *23*, 329–336.

Folkman, J., and Shing, Y. (1992). Angiogenesis. J. Biol. Chem. *267*, 10931–10934.

Gajiwala, K.S., Wu, J.C., Christensen, J., Deshmukh, G.D., Diehl, W., DiNitto, J.P., English, J.M., Greig, M.J., He, Y.A., Jacques, S.L., et al. (2009). KIT kinase mutants show unique mechanisms of drug resistance to imatinib and sunitinib in gastrointestinal stromal tumor patients. Proc. Natl. Acad. Sci. U S A *106*, 1542–1547.

Garner, A.P., Gozgit, J.M., Anjum, R., Vodala, S., Schrock, A., Zhou, T., Serrano, C., Eilers, G., Zhu, M., Ketzer, J., et al. (2014). Ponatinib inhibits polyclonal drug-resistant KIT oncoproteins and shows therapeutic potential in heavily pretreated gastrointestinal stromal tumor (GIST) patients. Clin. Cancer Res. *20*, 5745–5755.

George, S., Heinrich, M.C., Razak, A.R.A., Chi, P., Gordon, M.S., Ganjoo, K.N., Mehren, M.V., Somaiah, N., Trent, J.C., Su, Y., et al. (2018). Mutation profile of drug resistant gastrointestinal stromal tumor (GIST) patients (pts) enrolled in the phase 1 study of DCC-2618. J. Clin. Oncol. *36*, 11511.

Gotlib, J., Kluin-Nelemans, H.C., George, T.I., Akin, C., Sotlar, K., Hermine, O., Awan, F.T., Hexner, E., Mauro, M.J., Sternberg, D.W., et al. (2016). Efficacy and safety of midostaurin in advanced systemic mastocytosis. N. Engl. J. Med. *374*, 2530–2541.

Gounder, M.M., and Maki, R.G. (2011). Molecular basis for primary and secondary tyrosine kinase inhibitor resistance in gastrointestinal stromal tumor. Cancer Chemother. Pharmacol. *67* (*Suppl 1*), S25–S43.

Hanahan, D., and Coussens, L.M. (2012). Accessories to the crime: functions of cells recruited to the tumor microenvironment. Cancer Cell *21*, 309–322.

Harney, A.S., Karagiannis, G.S., Pignatelli, J., Smith, B.D., Kadioglu, E., Wise, S.C., Hood, M.M., Kaufman, M.D., Leary, C.B., Lu, W.P., et al. (2017). The selective Tie2 inhibitor rebastinib blocks recruitment and function of Tie2Hi macrophages in breast cancer and pancreatic neuroendocrine tumors. Mol. Cancer Ther. *16*, 2486–2501.

Heinrich, M.C., Corless, C.L., Blanke, C.D., Demetri, G.D., Joensuu, H., Roberts, P.J., Eisenberg, B.L., von Mehren, M., Fletcher, C.D., Sandau, K., et al. (2006). Molecular correlates of imatinib resistance in gastrointestinal stromal tumors. J. Clin. Oncol. *24*, 4764–4774.

Heinrich, M.C., Corless, C.L., Demetri, G.D., Blanke, C.D., von Mehren, M., Joensuu, H., McGreevey, L.S., Chen, C.J., Van den Abbeele, A.D., Druker, B.J., et al. (2003a). Kinase mutations and imatinib response in patients with metastatic gastrointestinal stromal tumor. J. Clin. Oncol. *21*, 4342–4349.

Heinrich, M.C., Corless, C.L., Duensing, A., McGreevey, L., Chen, C.J., Joseph, N., Singer, S., Griffith, D.J., Haley, A., Town, A., et al. (2003b). PDGFRA activating mutations in gastrointestinal stromal tumors. Science *299*, 708–710.

Heinrich, M.C., Griffith, D.J., Druker, B.J., Wait, C.L., Ott, K.A., and Zigler, A.J. (2000). Inhibition of c-kit receptor tyrosine kinase activity by STI 571, a selective tyrosine kinase inhibitor. Blood *96*, 925–932.

Heinrich, M.C., Maki, R.G., Corless, C.L., Antonescu, C.R., Harlow, A., Griffith, D., Town, A., McKinley, A., Ou, W.B., Fletcher, J.A., et al. (2008). Primary and secondary kinase genotypes correlate with the biological and clinical activity of sunitinib in imatinib-resistant gastrointestinal stromal tumor. J. Clin. Oncol. *26*, 5352–5359.

Hu, J., Ahuja, L.G., Meharena, H.S., Kannan, N., Kornev, A.P., Taylor, S.S., and Shaw, A.S. (2015). Kinase regulation by hydrophobic spine assembly in cancer. Mol. Cell. Biol. *35*, 264–276.

Huse, M., and Kuriyan, J. (2002). The conformational plasticity of protein kinases. Cell *109*, 275–282.

Janku, F., Razak, A.R.A., Gordon, M.S., Flynn, D., Kaufman, M., Pitman, J., Smith, B., Somaiah, N., Jennings, J., Salah, S., et al. (2017). Encouraging activity of novel pan-KIT and PDGFRα inhibitor DCC-2618 in patients (pts) with gastrointestinal stromal tumor (GIST). Ann. Oncol. *28*, mdx387.

Joensuu, H., Puputti, M., Sihto, H., Tynninen, O., and Nupponen, N.N. (2005). Amplification of genes encoding KIT, PDGFRalpha and VEGFR2 receptor tyrosine kinases is frequent in glioblastoma multiforme. J. Pathol. *207*, 224–231.

Joensuu, H., Roberts, P.J., Sarlomo-Rikala, M., Andersson, L.C., Tervahartiala, P., Tuveson, D., Silberman, S., Capdeville, R., Dimitrijevic, S., Druker, B., and Demetri, G.D. (2001). Effect of the tyrosine kinase inhibitor STI571 in a patient with a metastatic gastrointestinal stromal tumor. N. Engl. J. Med. *344*, 1052–1056.

Joyce, J.A. (2005). Therapeutic targeting of the tumor microenvironment. Cancer Cell *7*, 513–520.

Kemmer, K., Corless, C.L., Fletcher, J.A., McGreevey, L., Haley, A., Griffith, D., Cummings, O.W., Wait, C., Town, A., and Heinrich, M.C. (2004). KIT mutations are common in testicular seminomas. Am. J. Pathol. *164*, 305–313.

Klug, L.R., Kent, J.D., and Heinrich, M.C. (2018). Structural and clinical consequences of activation loop mutations in class III receptor tyrosine kinases. Pharmacol. Ther. *191*, 123–134.

Lasho, T., Finke, C., Zblewski, D., Hanson, C.A., Ketterling, R.P., Butterfield, J.H., Tefferi, A., and Pardanani, A. (2016). Concurrent activating KIT mutations in systemic mastocytosis. Br. J. Haematol. *173*, 153–156.

Lebedev, A.A., Young, P., Isupov, M.N., Moroz, O.V., Vagin, A.A., and Murshudov, G.N. (2012). JLigand: a graphical tool for the CCP4 template-restraint library. Acta Crystallogr D. Biol. Crystallogr *68*, 431–440.

Liegl, B., Kepten, I., Le, C., Zhu, M., Demetri, G.D., Heinrich, M.C., Fletcher, C.D., Corless, C.L., and Fletcher, J.A. (2008). Heterogeneity of kinase inhibitor resistance mechanisms in GIST. J. Pathol. *216*, 64–74.

Malaise, M., Steinbach, D., and Corbacioglu, S. (2009). Clinical implications of c-Kit mutations in acute myelogenous leukemia. Curr. Hematol. Malig. Rep. *4*, 77–82.

McCoy, A.J., Grosse-Kunstleve, R.W., Adams, P.D., Winn, M.D., Storoni, L.C., and Read, R.J. (2007). Phaser crystallographic software. J. Appl. Crystallogr *40*, 658–674.

Melnick, J.S., Janes, J., Kim, S., Chang, J.Y., Sipes, D.G., Gunderson, D., Jarnes, L., Matzen, J.T., Garcia, M.E., Hood, T.L., et al. (2006). An efficient rapid system for profiling the cellular activities of molecular libraries. Proc. Natl. Acad. Sci. U S A *103*, 3153–3158.

Mol, C.D., Dougan, D.R., Schneider, T.R., Skene, R.J., Kraus, M.L., Scheibe, D.N., Snell, G.P., Zou, H., Sang, B.C., and Wilson, K.P. (2004). Structural basis for the autoinhibition and STI-571 inhibition of c-Kit tyrosine kinase. J. Biol. Chem. *279*, 31655–31663.

Murshudov, G.N., Skubak, P., Lebedev, A.A., Pannu, N.S., Steiner, R.A., Nicholls, R.A., Winn, M.D., Long, F., and Vagin, A.A. (2011). REFMAC5 for the refinement of macromolecular crystal structures. Acta Crystallogr D. Biol. Crystallogr *67*, 355–367.

Nagata, H., Worobec, A.S., Oh, C.K., Chowdhury, B.A., Tannenbaum, S., Suzuki, Y., and Metcalfe, D.D. (1995). Identification of a point mutation in the catalytic domain of the protooncogene c-kit in peripheral blood mononuclear cells of patients who have mastocytosis with an associated hematologic disorder. Proc. Natl. Acad. Sci. U S A *92*, 10560–10564.

Paschka, P., Marcucci, G., Ruppert, A.S., Mrozek, K., Chen, H., Kittles, R.A., Vukosavljevic, T., Perrotti, D., Vardiman, J.W., Carroll, A.J., et al. (2006). Adverse prognostic significance of KIT mutations in adult acute myeloid leukemia with inv(16) and t(8;21): a cancer and leukemia group B study. J. Clin. Oncol. *24*, 3904–3911.

Peter, B., Winter, G.E., Blatt, K., Bennett, K.L., Stefanzl, G., Rix, U., Eisenwort, G., Hadzijusufovic, E., Gridling, M., Dutreix, C., et al. (2016). Target interaction profiling of midostaurin and its metabolites in neoplastic mast cells predicts distinct effects on activation and growth. Leukemia *30*, 464–472.

Ramos, A.H., Dutt, A., Mermel, C., Perner, S., Cho, J., Lafargue, C.J., Johnson, L.A., Stiedl, A.C., Tanaka, K.E., Bass, A.J., et al. (2009). Amplification of chromosomal segment 4q12 in non-small cell lung cancer. Cancer Biol. Ther. *8*, 2042–2050.

Rubin, B.P., Singer, S., Tsao, C., Duensing, A., Lux, M.L., Ruiz, R., Hibbard, M.K., Chen, C.J., Xiao, S., Tuveson, D.A., et al. (2001). KIT activation is a ubiquitous feature of gastrointestinal stromal tumors. Cancer Res. *61*, 8118–8121.

Serrano, C., and George, S. (2014). Recent advances in the treatment of gastrointestinal stromal tumors. Ther. Adv. Med. Oncol. *6*, 115–127.

Sundstrom, M., Vliagoftis, H., Karlberg, P., Butterfield, J.H., Nilsson, K., Metcalfe, D.D., and Nilsson, G. (2003). Functional and phenotypic studies of two variants of a human mast cell line with a distinct set of mutations in the c-kit proto-oncogene. Immunology *108*, 89–97.

Verhaak, R.G., Hoadley, K.A., Purdom, E., Wang, V., Qi, Y., Wilkerson, M.D., Miller, C.R., Ding, L., Golub, T., Mesirov, J.P., et al. (2010). Integrated genomic analysis identifies clinically relevant subtypes of glioblastoma characterized by abnormalities in PDGFRA, IDH1, EGFR, and NF1. Cancer Cell *17*, 98–110.

Verstovsek, S. (2013). Advanced systemic mastocytosis: the impact of KIT mutations in diagnosis, treatment, and progression. Eur. J. Haematol. *90*, 89–98.

Wodicka, L.M., Ciceri, P., Davis, M.I., Hunt, J.P., Floyd, M., Salerno, S., Hua, X.H., Ford, J.M., Armstrong, R.C., Zarrinkar, P.P., and Treiber, D.K. (2010). Activation state-dependent binding of small molecule kinase inhibitors: structural insights from biochemistry. Chem. Biol. *17*, 1241–1249.

Wyckoff, J.B., Wang, Y., Lin, E.Y., Li, J.F., Goswami, S., Stanley, E.R., Segall, J.E., Pollard, J.W., and Condeelis, J. (2007). Direct visualization of macrophage-assisted tumor cell intravasation in mammary tumors. Cancer Res. *67*, 2649–2656.

STAR★METHODS

KEY RESOURCES TABLE

REAGENT or RESOURCE	SOURCE	IDENTIFIER
Antibodies		
AKT; rabbit polyclonal	Cell Signaling	Cat#9272; RRID:AB_329827
Anti-phosphotyrosine-HRP; mouse monoclonal	Life Technologies	Cat#03-7720; RRID:AB_2532960
CSF1R; mouse monoclonal	R&D Systems	Cat#MAB3292; RRID:AB_2085247
ERK1/2; rabbit polyclonal	Cell Signaling	Cat#9102; RRID:AB_330744
Human Phospho-VEGFR2 ELISA kit (VEGFR2 capture antibody; phosphotyrosine-HRP antibody)	R&D Systems	Cat#DYC1766
KIT (C-19); rabbit polyclonal	Santa Cruz	Cat#sc-168; RRID:AB_631033
KIT; rabbit monoclonal	Cell Signaling	Cat#3074; RRID:AB_1147633
PDGFRA (C-20); rabbit polyclonal	Santa Cruz	Cat#sc-338; RRID:AB_631064
PDGFRA; rabbit polyclonal	Cell Signaling	Cat#3164; RRID:AB_631064
Phospho-AKT (Ser473); rabbit monoclonal	Cell Signaling	Cat#4058; RRID:AB_331168
Phospho-ERK1/2; rabbit polyclonal	Cell Signaling	Cat#9101; RRID:AB_331646
Phospho-KIT (Tyr703); rabbit monoclonal	Cell Signaling	Cat#3073; RRID:AB_1147635
Phospho-Kit (Tyr719) ELISA Kit (mouse monoclonal KIT capture antibody; rabbit monoclonal phospho-KIT antibody)	Cell Signaling	Cat#7299; RRID:AB_10693164
Phospho-KIT (Tyr719); rabbit polyclonal	Cell Signaling	Cat#3391; RRID:AB_2131153
Phospho-PDGFRA (Tyr754); rabbit monoclonal	Cell Signaling	Cat#2992; RRID:AB_390728
Phospho-PDGFRA ELISA kit (mouse PDGFRA capture antibody; mouse phosphotyrosine-HRP antibody)	R&D Systems	Cat#DYC2114
Phospho-PDGFRB Tyr751 ELISA kit (goat PDGFRB capture antibody; rabbit phospho-PDGFRB antibody)	R&D Systems	Cat#DYC3096
Phospho-STAT5 (Tyr694); rabbit polyclonal	BD Biosciences	Cat#611819; RRID:AB_399299
Phospho-TIE2 (Tyr992); rabbit polyclonal	Cell Signaling	Cat#4221; RRID:AB_2203198
Phospho-tyrosine (PY20); mouse monoclonal	BD Transduction Labs	Cat#610000; RRID:AB_397423
STAT5; rabbit polyclonal	Cell Signaling	Cat#9363; RRID:AB_10693321
TIE2 (C-20); rabbit polyclonal	Santa Cruz	Cat#sc-324; RRID:AB_631102
Biological Samples		
Xenograft tumor samples	MI Bioresearch	https://www.mibioresearch.com
Patient-derived xenograft tumor samples	Molecular Response	https://Molecularresponse.com
Chemicals, Peptides, and Recombinant Proteins		
ABL L248-T534 with N-terminal His-tag	DeCode Biostructures	https://be4.com
Abltide (EAIYAAPFAKKK-OH) for ABL and ARG assays	Biopeptide Co.	https://www.biopeptide.com
ACK	SignalChem	Cat#A05-11G
AKT	Millipore	Cat#14-453
ARAF	BPS Bioscience	Cat#40010
ARG	Invitrogen	Cat#PV3266
BLU-285	SelleckChem	Cat#S8553-02
BLU-285	This paper	N/A
BRK	SignalChem	Cat#P94-10G
Crosstide (GRPRTSSFAEG-OH) for AKT assays	Biopeptide Co.	https://www.biopeptide.com
CSF1R	Millipore	Cat#14-551
CSK	SignalChem	Cat#C63-10G
DCC-2618	This paper	N/A
DDR2	SignalChem	Cat#D06-11BG

(*Continued on next page*)

Continued

REAGENT or RESOURCE	SOURCE	IDENTIFIER
DP-2976	This paper	N/A
DP-5439	This paper	N/A
EPHA1	SignalChem	Cat#E13-11G
EPHA2	SignalChem	Cat#E14-11G
EPHA3	SignalChem	Cat#E15-11G
EPHA4	SignalChem	Cat#E16-11G
EPHA5	Carna Bio	Cat#8-124
EPHA8	Carna Bio	Cat#8-127
EPHB1	SignalChem	Cat#E21-11G
EPHB2	SignalChem	Cat#E22-11G
FGFR1	Invitrogen	Cat#PV-3146
FGR	Invitrogen	Cat#P-3041
FLT1	SignalChem	Cat#G11-11G
FLT3	Invitrogen	Cat#PV-3182
FLT4	CarnaBio	Cat#08-190
FMS	Millipore	Cat#14-551
FRK	SignalChem	Cat#F14-11G
FYN	Invitrogen	Cat#P-3042
HCK	Invitrogen	Cat#P-2908
HER1	Invitrogen	Cat#PV-4190
HIPK4	SignalChem	Cat#H06-10G
IKK-A	SignalChem	Cat#C51-10G
Imatinib	This paper	N/A
IRK residues S981-K1283	DeCode Biostructures	https://be4.com
JAK2	Invitrogen	Cat#PV-4288
JNK1	SignalChem	Cat#M33-10G
JNK2	SignalChem	Cat#M34-10BG
KDR residues D807-K939 and A991-D1171	DeCode Biostructures	https://be4.com
KHS1	SignalChem	Cat#M27-10G
KIT kinase and V654A, T670I, D816H, D816V, and ΔV559-V560/D816V variants; T544-V976, N-terminal His-Glu-GST-TEV tag/cleavage	DeCode Biostructures	https://be4.com
LCK	Invitrogen	Cat#P-3043
LOK	SignalChem	Cat#S29-11G
LYN	Invitrogen	Cat#P-2906
MEK1 M1-V393	DeCode Biostructures	https://be4.com
MEKK3	SignalChem	Cat#M11-10G
MELK	SignalChem	Cat#M50-18G
MET T1050-K1360; N-term His-Glu-TEV tag/cleavage	DeCode Biostructures	https://be4.com
Midostaurin	LC Laboratories	Cat#P-7600
MK2	Invitrogen	Cat#PV-3317
MK2 peptide (KKLNRTLSVA-NH2)	Biopeptide Co.	https://www.biopeptide.com
MLK1	SignalChem	Cat#M17-11G
MLK2	SignalChem	Cat#M18-11G
MLK3	SignalChem	Cat#M19-11G
MYLK2	SignalChem	Cat#M63-10H
p38 peptide (IPTSPITTTYFFFKKK-OH)	Biopeptide Co.	https://www.biopeptide.com
p38a M1-S360	DeCode Biostructures	https://be4.com
p38b M1-Q364	DeCode Biostructures	https://be4.com

(*Continued on next page*)

Continued

REAGENT or RESOURCE	SOURCE	IDENTIFIER
PDGFRA; K550-L1089, N-terminal His-GST fusion tag	DeCode Biostructures	https://be4.com
PDGFRB; Q557-L1106, N-terminal His-GST fusion tag	DeCode Biostructures	https://be4.com
PDGFRα D842V	Invitrogen/Life Technologies	Cat#PV4203
PolyEY	Sigma	Cat#P7244
Recombinant ANG-1	R&D Systems	Cat#923-AN
Recombinant human MCSF	R&D Systems	Cat#216-MC
Recombinant human VEGF	R&D Systems	Cat#293-VE
Regorafenib	This paper	N/A
Resazurin	Sigma	Cat#R7017
RET	Invitrogen	Cat#PV-3819
SLK	SignalChem	Cat#S11-10G
SRC M1-L536 with C-term His-tag	DeCode Biostructures	https://be4.com
Sunitinib	LC Laboratories	Cat#S-8803
TAK1-TAB1	SignalChem	Cat#M15-13G
TAOK1	SignalChem	Cat#T24-11G
TAOK2	SignalChem	Cat#T25-11G
TAOK3	SignalChem	Cat#T26-11G
TIE2	SignalChem	Cat#T04-11g
TRKA	Invitrogen	Cat#PV-3144
TRKC	Carna Bio	Cat#08-197
YES	SignalChem	Cat#Y01-10G
ZAK	SignalChem	Cat#Z01-10G
Critical Commercial Assays		
Kinase panel activity assays	Reaction Biology Corporation	http://www.reactionbiology.com
Kinase binding assays (KdELECT)	DiscoverX	https://www.discoverx.com
Guardant360	Guardant Health	https://www.guardanthealth.com/guardant360
Deposited Data		
KIT:DP-2976 structure	This paper	PDB: 6MOB
Experimental Models: Cell Lines		
Hamster: CHO-K1	ATCC	Cat#CCL-61; RRID:CVCL_0214
Human: A375	ATCC	Cat#CRL-1619; RRID:CVCL_0132
Human: GIST T1 (KIT exon 11 deletion)	Dr. Brian Rubin	RRID:CVCL_4976
Human: GIST T1 5R (KIT exon 11 deletion / exon 14 T670I	Dr. Brian Rubin	N/A
Human: GIST T1 Juke (KIT exon 11 deletion / exon 17 D816E	Dr. Brian Rubin	N/A
Human: GIST430 (KIT exon 11 deletion / exon 13 V654A)	Dr. Jonathan Fletcher	N/A
Human: GIST48 (KIT exon 11 V560D / exon 17 D820A)	Dr. Jonathan Fletcher	RRID:CVCL_7041
Human: GIST882 (KIT exon 13 K642E)	Dr. Jonathan Fletcher	RRID:CVCL_7044
Human: H1703	ATCC	Cat#CRL-5889; RRID:CVCL_1490
Human: HCT-116	ATCC	Cat#CCL-247; RRID:CVCL_0291
Human: HMC1.1 (KIT exon 11 V560G)	Millipore	Cat#SCC067; RRID:CVCL_H206
Human: HMC1.2 (KIT exon 11 V560G / exon 17 D816V)	Millipore	Cat#SCC062; RRID:CVCL_H205
Human: HUVEC	Fisher	Cat#NC994667
Human: HUVEC	ATCC	Cat#CRL-1730; RRID:CVCL_2959
Human: Kasumi (KIT N822K)	ATCC	Cat#CRL-2724; RRID:CVCL_0589
Human: MV-4-11	ATCC	Cat#CRL-9591; RRID:CVCL_0064

(*Continued on next page*)

Continued

REAGENT or RESOURCE	SOURCE	IDENTIFIER
Human: REN	Dr. Steven Albelda	RRID:CVCL_M202
Human: THP-1	ATCC	Cat#TIB-202; RRID:CVCL_0006
Mouse: Ba/F3 (Heinrich laboratory)	Dr. Michael Heinrich	N/A
Mouse: Ba/F3 (Deciphera Pharmaceuticals)	Dr. Richard Van Etten	N/A
Mouse: P815 (KIT D814Y)	ATCC	Cat#TIB-64; RRID:CVCL_2154
Experimental Models: Organisms/Strains		
Mouse: Hsd:Athymic Nude-Foxn1^{nu}	Envigo	https://www.envigo.com; RRID:MGI:5652489
Mouse: NOD.SCID (NOD.CB17-*Prkdc*^{scid}/NCrHsd)	Envigo	https://www.envigo.com
Mouse: BALB/cOlaHsd-Foxn1^{nu}	Charles River	https://www.criver.com
Mouse: Crl:NU-Foxn1^{nu}	Charles River	https://www.criver.com; RRID:IMSR_CRL:088
Oligonucleotides		
KIT-exon-8F- CAAAACCAGAAATCCTGACTTACGA	This paper	N/A
KIT-exon-21R- CATCGTCGTGCACAAGCAGA GGCTG	This paper	N/A
KIT-exon-15F- CAGCGATAGTACTAATGAGTACATG	This paper	N/A
KIT-exon-16R-TGGCGGGAGTCACATCTC TTTCTATG	This paper	N/A
Recombinant DNA		
pcDNA3.2/V5-DEST vector	Invitrogen	Cat#12489-019
pcDNA3.1	Invitrogen	Cat#V79020
pDNR-CMV	Clontech	Cat#639602
Software and Algorithms		
Prism 7	GraphPad	https://ww.graphpad.com
ImageQuant TL	GE Healthcare	https://www.gehealthcare.com
Photoshop 5.1	Adobe	https://www.adobe.com
Calcusyn 2.1	Biosoft	http://www.biosoft.com
PHASER	McCoy et al., 2007	http://www.ccp4.ac.uk
COOT	Emsley et al., 2010	http://www2.mrc-lmb.cam.ac.uk/personal/pemsley/coot
REFMAC5	Murshudov et al., 2011	http://www.ccp4.ac.uk
JLigand	Lebedev et al., 2012	http://www.ccp4.ac.uk
Other		
Fetal Bovine Serum; Certified US Origin	Life Technologies	Cat#16000-044
Lipofectamine® LTX Reagent with PLUS™ Reagent	Life Technologies	Cat#15338-100
Bovine Pituitary Extract	BD Biosciences	Cat#356123
Mito+ Serum Extender	BD Biosciences	Cat#355006

CONTACT FOR REAGENT AND RESOURCE SHARING

Further information and requests for resources and reagents should be directed to and will be fulfilled by the Lead Contact, Daniel L. Flynn (dflynn@deciphera.com). MTAs will be required for any materials used in the study. Some information or data linked to sensitive medical information may not be shared.

EXPERIMENTAL MODEL AND SUBJECT DETAILS

Human Subjects

The safety and tolerability of ripretinib was tested in a First-in-Human study (NCT02571036). The study was reviewed and approved by the institutional review boards at the University of Texas MD Anderson Cancer Center and Princess Margaret Cancer Centre. Written informed consent was obtained from all patients before study entry. Two patients enrolled during the dose escalation phase of the

study are described herein. Patient 1 was a 62-year-old male 4th line GIST patient who progressed on all approved treatment options (i.e., imatinib, sunitinib, and regorafenib) prior to enrollment in the study. The patient was enrolled in the 50 mg BID dose escalation cohort. Patient 2 was a 56-year-old female 4th line GIST patient who progressed on all approved TKIs (i.e., imatinib, sunitinib, and regorafenib) prior to enrollment in the study. The patient was enrolled into the 150 mg BID dose escalation cohort.

Mouse Models

The GIST T1, H1703, HMC1.2, P815 and MTD studies were performed in compliance with all the laws, regulations and guidelines of the National Institutes of Health (NIH) and with the approval of the Animal Care and Use Committee of Molecular Imaging, Inc. or MI Bioresearch (Ann Arbor, MI), AAALAC accredited facilities. Mice were housed in Innovive disposable ventilated caging with corn cob bedding inside Biobubble® Clean Rooms, with 1-5 mice per cage. The light cycle was 12 hr light/12 hr dark, with temperature at 70±2°F, and humidity at 30-70%. The GIST PDX model was performed in compliance with the U.S. Department of Agriculture's Animal Welfare Act (9 CFR Parts 1, 2, and 3), as applicable. For the GIST PDX model, all experimental data management and reporting procedures were in strict accordance with applicable Molecular Response, LLC's Guidelines and Standard Operating Procedures. Animals were housed in individual HEPA ventilated cages (Innocage® IVC, Innovive USA). Fluorescent lighting was provided on a 12-hour cycle. Temperature and humidity was monitored and recorded daily and maintained to the maximum extent possible between 68-74°F (20-23°C) and 30-70% humidity, respectively. All mice in all studies had food and water *ad libitum.* All mice in all studies were observed for clinical signs at least once daily. Tumor volume and body weight were measured thrice weekly. Tumor burden (mg) was estimated from caliper measurements by the formula: tumor burden ($mg=mm^3$) = (length x $width^2$)/2. For tumor model studies, mice were randomly assigned to groups, achieving similar mean tumor burden for each cohort on the first day of dosing.

For the GIST T1 xenograft study, female nude mice (Hsd:Athymic Nude-Foxn1^{nu}; Envigo; 6-7 weeks old) were acclimated for 7 days after arrival. The mean weight of groups of mice ranged from 22.1-24.1 g on the first day of dosing. For the GIST PDX KIT exon 11 deletion / exon 17 Y823D model, female NOD-SCID mice (Harlan Laboratories; 6-7 weeks old) were acclimated for 3 days after arrival. The mean weight of groups of mice ranged from 22.9-24.0 g on the first day of dosing. For the P815 allograft model, female BALB/c nude mice (BALB/cOlaHsd-Foxn1^{nu}; Charles River; 7-8 weeks old) were acclimated for 3 days after arrival. The mean weight of groups of mice ranged from 15.7-16.9 g on the first day of dosing. For the HMC1.2 xenograft model, female nude mice (Hsd:Athymic Nude-Foxn1^{nu}; Envigo; 5-6 weeks old) were acclimated for 7 days after arrival. The mean weight of groups of mice ranged from 21.3-22.2 g on the first day of dosing. For the H1703 xenograft model, female nude mice (Hsd:Athymic Nude-Foxn1^{nu}; Envigo; 6-7 weeks old) were acclimated for 7 days after arrival. The mean weight of groups of mice ranged from 19.8-21.3 g on the first day of dosing. For the GIST T1 xenograft mouse pharmacokinetic/pharmacodynamic dose models, female nude mice (Crl:NU-Foxn1^{nu}; Charles River; 8-9 weeks old) were acclimated for 7 days after arrival. The mean weight of groups of mice ranged from 21.3-22.2 g on the first day of dosing. For the MTD study, female nude mice (Crl:NU-Foxn1^{nu}; Charles River; 11-2 weeks old) were acclimated for 5 days after arrival. Mice were randomized into groups such that the mean weight of groups of mice were within 10% of the overall mean. Mean group weights ranged from 23.2-23.6 g on the first day of dosing.

Cell Lines and Culture Conditions

CHO-K1 (female Chinese hamster ovary), HUVECs (human umbilical vein endothelial cells, various lots, sex not known), H1703 (male human lung cancer), Kasumi-1 (male human acute myeloblastic leukemia), P815 (male mouse mastocytoma), THP-1 (male human acute monocytic leukemia), MV-4-11 (male human leukemia), A375 (female human malignant melanoma), and HCT-116 (male human colorectal cancer) cells were purchased from the American Type Culture Collection (ATCC, Manassas, VA). EOL1 (male human eosinophilic leukemia cells), HMC1.1 (male human mast cell leukemia), and HMC1.2 (HMC1.1 subclone with secondary D816V KIT mutation) cell lines were purchased from Millipore. Ba/F3 (mouse B cells, sex not available) cells were received from R. Van Etten. REN (human malignant pleural mesothelioma, sex not available) cells were received from S. Albelda. GIST T1 (female human GIST), GIST T1 5R (subclone of GIST T1 with secondary T670I KIT mutation), and GIST T1 Juke (subclone of GIST T1 with secondary D816E KIT mutation) cells were received from B. Rubin. GIST48, GIST430, and GIST882 human GIST cell lines (sex not available) were received from J. Fletcher. All commercial cell lines were cultured as recommended by the supplier, unless otherwise indicated. Media was purchased from Life Technologies or Lonza, Inc. Generally, cells were cultured in media containing 10% characterized fetal bovine serum (FBS) and 1% Penicillin-streptomycin-L-glutamine (P/S/G). Cells were grown at 37°C with 90-95% humidity. GIST 430 cells were supplemented with 15% FBS, Bovine Pituitary Extract (BD Biosciences #356123) and Mito+ Serum Extender (BD Biosciences #355006). Cell lines were expanded upon receipt and then frozen at an early passage number in aliquots in liquid N_2. Cells were then passaged fewer than 6 months after resuscitation. HUVECs were passaged <10 times upon resuscitation. The ATCC and Millipore perform STR analysis for characterization. Further STR characterization was not performed. Mycoplasma testing was performed on a monthly basis for all cell lines (except for HUVECs), using the MycoAlert Detection Kit from Lonza, Inc.

Insect Cells

For crystallography studies, Tni PRO and Sf9 cells were from Expression Systems (Davis, CA; #94-004F and #94-001F, respectively). Cells were grown in ESF 921—protein-free insect cell culture medium from Expression Systems.

METHOD DETAILS

Chemical Synthesis

Ripretinib (DCC-2618) was synthesized as described in US patent 8461179B1, Example 31. DP-5439 was synthesized as described in US patent 8461179B1, Example 57. DP-2976 was synthesized as described in WO2008034008, Example 276. BLU-285 was synthesized according to methods in patent WO2015057873; example 7, compound 44; and the racemic mixture was purified via preparatory chiral HPLC chomatography (Chiralpak IB-4.6x250, 100% EtOH). The two enantiomers were isolated with retention times of 9.79 and 11.87 minutes, respectively. The two enantiomers were assayed for biological activity in multiple KIT and PDGFRA assays. The less polar enantiomer (Rt = 9.79 minutes) was found to be the most potent and was assigned as BLU-285. To confirm, the (*S*)-enantiomer of BLU-285 was also purchased from Selleckchem. This material was found to have the same retention time as the less polar enantiomer, and co-injection indicated that the compounds were identical.

Protein Production for Crystallograpy

Expression Vector Design

A synthetic gene containing the KIT kinase domain beginning at amino acid 565 and ending at amino acid 935 with a deletion of the kinase insert domain region Q694-T753 was obtained from DNA2.0 (ATUM, Newark, CA). The coding region was subcloned by PCR into baculovirus transfer vector pBacGus-1 (EMD/Novagen, MA). Following amplification, the PCR product was digested with BamHI and HindIII (Fermentas) and subcloned into BamHI/HindIII-digested pBacgus-1, and the ORF from a single transformed clone was sequence verified.

Expression and Purification of KIT (565-935, ΔQ694-T753) Protein

The recombinant His-Glu tagged KIT (565-935, ΔQ694-T753) in pBacgus-1 was transfected into Trichoplusia ni (Tni) insect cells along with BestBac genomic baculo virus DNA (Expression Systems, Davis, CA). The resulting recombinant baculovirus was amplified to produce P3/P4 virus stocks in Sf9 cells. This virus stock was used for all large-scale infections. Large scale infections were done in Tni cells and typically 5 to 8 fernbach volumes were infected to produce cell paste for KIT (565-935, ΔQ694-T753) purifications. Purification was completed on cell paste that was cultured with 5 μM DP-2976 during growth. The His-Glu tagged KIT (565-935, ΔQ694-T753) was enriched from the Tni cell lysate by Ni affinity chromatography (Hi-Trap Chelating HP, GE Healthcare) then eluted from the Ni column in a buffer containing 20mM Tris pH 8.0, 250 mM NaCl, 500 mM imidazole and Complete™ EDTA-free protease inhibitors (Roche, IN). The N-terminal His-Glu affinity tag was cleaved from the KIT (565-935, ΔQ694-T753) protein domain by overnight incubation with TEV protease at 16°C. The pool was dialyzed against 20 mM Tris pH 8.0 for three hr and the KIT (565-935, ΔQ694-T753) domain was separated from the uncleaved protein and the His-Glu affinity tag by subtractive Ni chromatography. KIT (565-935, ΔQ694-T753) eluted during the wash step and was incubated for 48 hr with a five-molar excess of DP-2976 at which time the pool was sterile filtered and concentrated to 12 mg/mL for crystallography. The final buffer composition consisted of 20 mM Tris pH 8.0, 0.25 M NaCl, 5 mM imidazole, 5 mM DTT and 1 mM EDTA. All purification steps were performed at 4°C.

X-Ray Crystallography

Crystallization Conditions

Purified KIT (565-935, ΔQ694-T753)/DP-2976 was utilized at 12 mg/mL for crystallography and complex crystals were grown by the vapor diffusion method in sitting drops set up with a 0.5 μL/0.5 μL protein to crystallant drop ratio, the crystallant consisting of 2.5 M ammonium nitrate, 0.1 M sodium acetate pH 4.6.

Data Collection and Structure Refinement

An X-ray diffraction dataset was collected on the KIT (565-935, ΔQ694-T753)/DP-2976 complex crystal using synchrotron radiation at the Canadian Light Source (CLS; Saskatoon, Canada) synchrotron beamline I81 on September 17, 2009. A single dataset at 1.8 Å resolution was collected at a wavelength of 0.9795 Å. KIT (565-935, ΔQ694-T753)/DP-2976 crystallizes in space group $P4_32_12$ with unit cell dimensions $a=b=80.699$, $c=145.02$, $\alpha=\beta=\gamma=90^\circ$ with one molecule per asymmetric unit. The structure was determined using molecular replacement in the program PHASER (McCoy et al., J. Appl. Crys. (2007) 40, 658-674) and a previously solved structure of KIT (pdb 1T46) as the search model. The model was visualized and manipulated with COOT (Emsley et al., Acta Crystallogr. D Biol Crystallogr. (2010) 66, 486-501) and refined with REFMAC5 (Murshudov et al., Acta Crystallogr (2011) D67, 355-367) using ligand restraint generated with JLigand (Lebedev et al., Acta Cryst (2012) D68, 431-440). R_{work}=18.1 and R_{free}=21.0. Data set and refinement statistics are summarized in Table S1.

Kinase Assays

Kinase activity was determined by following the production of ADP from the kinase reaction through coupling with the pyruvate kinase/lactate dehydrogenase system. In this assay, the oxidation of NADH (resulting in a decrease in absorbance at 340 nm) was continuously monitored spectrophotometrically at 30°C on a plate reader. Assays were conducted in 384-well plates (100 μL final volume) using enzyme, 1.5 units pyruvate kinase, 2.1 units lactate dehydrogenase, 1 mM phosphoenol pyruvate, 0.28 mM NADH, and 1 mg/mL PolyEY in assay buffer (100 mM Tris, pH 7.5, 15 mM $MgCl_2$, 0.5 mM DTT, 0.1% octyl-glucoside, 0.002% (w/v) BSA, and 0.002% Triton X-100). Assay mixtures were mixed with test compound diluted in buffer in 384-well plates. ATP was added into the assay mixture to start the reaction immediately. The absorbance at 340 nm was determined on a plate reader at 30°C every 2 min for up to 8 hr. Percent inhibition values were obtained by comparison of reaction rates with DMSO controls. IC_{50} values were

calculated from a series of percent inhibition values determined at a range of inhibitor concentrations using Prism software (GraphPad, San Diego, CA). For screening of a large kinase panel and the KIT mutant kinase panel at 10 μM ATP, assays were performed at Reaction Biology Corp. (Malvern, PA) using published methods (Anastassiadis et al., 2011). Competitive binding assays were performed at DiscoverX Corporation (Fremont, CA), using published methods (Fabian et al., 2005).

Cell Proliferation Assays

A serial dilution of test compound in DMSO was dispensed into 96- or 384-well black, clear bottom, tissue-culture treated plates (Corning, Corning, NY) in triplicate. Cells in complete culture media were added to the plates and the final concentration of DMSO in all assays was 0.5%. Plates were incubated for 72 h. Viable cells were quantified by addition of a 440 μM solution of resazurin in D-PBS. Plates were read on a fluorescent plate reader using an excitation of 540 nm and an emission of 600 nm. Data was analyzed using Prism software (GraphPad, San Diego, CA) to calculate IC_{50} values.

Enzyme-Linked Immunosorbent assays

Cells were added to 24-well tissue-culture treated plates and incubated overnight. Transfection-grade plasmid DNA was mixed with Lipofectamine LTX Reagent with PLUS Reagent (Life Technologies) and added to cells. Eighteen hr post-transfection, medium was aspirated, cells were washed, and serum-free medium was added. Test compound was added to plates and incubated for 4 hr. Cells were then lysed and phospho-KIT was detected using a human phospho-KIT ELISA (catalog #7299; Cell Signaling).

HUVECs in EBM-2 containing 2% FBS were plated in 96-well tissue-culture treated plates at 25,000 cells/well. Cells were incubated overnight, and diluted compound was then added to plates. Cells were incubated for 4 h, and stimulated with 100 ng/mL VEGF (catalog #293-VE, R&D Systems, Minneapolis, MN) for 5 min. Phospho-VEGFR2 in cell lysates was detected using the DuoSet IC Human Phospho-VEGFR2 ELISA (catalog #DYC1766, R&D Systems, Minneapolis, MN). For the phospho-FMS ELISA, THP-1 cells in RPMI 1640 containing 10% FBS were added to a 96-well plate containing diluted compound at 150,000 cells/well. Cells were incubated 4 h and then stimulated with 25 ng/mL MCSF (catalog #216-MC, R&D Systems, Minneapolis, MN) for 5 min prior to lysis. Phospho-FMS in cell lysates was detected using an anti-FMS capture antibody (catalog #MAB3292, R&D Systems) and an anti-phospho-tyrosine detection antibody conjugated to horseradish peroxidase (HRP; catalog #03-7720, Life Technologies).

Western Blot Assays

For CHO cell assays, cells were added to 24-well tissue-culture treated plates and incubated overnight. Transfection-grade plasmid DNA was mixed with Lipofectamine LTX Reagent with PLUS Reagent (Life Technologies) and added to cells. Eighteen hr post-transfection, medium was aspirated, cells were washed, and serum-free medium was added. Test compound was added to plates and incubated for 4 hr. Cells were then lysed. For other cell assays, cells in culture media were added to 24-well tissue-culture treated plates and incubated overnight. A serial dilution of test compound in DMSO was added and cells were incubated for an additional 4 h. The final concentration of DMSO in the assays was 0.5%. Cells were lysed in MPER buffer (Pierce, Rockford, IL) containing HALT protease and phosphatase inhibitors (Pierce, Rockford, IL) and Phosphatase Inhibitor Cocktail 2 (Sigma, St. Louis, MO). Protein was quantified using the Coomassie Plus Protein Assay Reagent (Pierce, Rockford, IL) using BSA as a standard. Equal protein amounts and MagicMark XP molecular weight markers (Invitrogen, Carlsbad, CA) were loaded onto NuPAGE 4→12% gradient polyacrylamide gels (Invitrogen, Carlsbad, CA). Proteins were transferred to PVDF membranes. Blots were probed using phospho-specific antibodies and HRP-conjugated secondary antibodies. Blots were stripped and probed with the corresponding total antibodies. Bands were detected using ECL Plus (GE Healthcare, Piscataway, NJ) and a Molecular Devices Storm 840 phosphorimager in fluorescence detection mode. Band volumes were quantified using ImageQuant software (GE Healthcare, Piscataway, NJ). For BaF3 cell studies, cells that had been stably transfected with mutated *PDGFRA* cDNA constructs were treated with various concentrations of compound for 90 minutes. Protein lysates from cells were prepared and subjected to immunoprecipitation using anti-PDGFRA antibody (SC-20, Santa Cruz Biotechnology, Santa Cruz, CA) and Protein A/G beads (Santa Cruz Biotechnology, Santa Cruz, CA), followed by sequential immunoblotting for phosphotyrosine using a monoclonal antibody (PY-20, BD Transduction Labs, Sparks, MD) or total PDGFRA (C-20, Santa Cruz Biotechnology, Santa Cruz, CA). Densitometry was performed to quantify drug effect using Photoshop 5.1 software, with the level of phospho-PDGFRA normalized to total protein. Densitometry experimental results were analyzed using Calcusyn 2.1 software (Biosoft, Cambridge, UK) to mathematically determine the IC_{50} values.

Saturation Mutagenesis

Ba/F3 cells stably transfected with V560D KIT kinase were treated with the mutagen ethylnitrosourea (ENU) for 18 hr. Cells were washed several times, and then cells were plated in wells containing various concentrations of ripretinib or imatinib. Wells showing growth were transferred to 24 well plates and grown in 2 mL of media for 2 days. DNA was isolated using Purelink Genomic DNA isolation Kit (Invitrogen, Carlsbad, CA). DNA was amplified by PCR. Briefly, 5 μL of PCR green buffer, 1.5 μL of $MgCl_2$, 1 μL of 10 mM dNTP, 1 μL of 10 μM primer KIT-exon-8F, 1 μL of 10 μM primer KIT-exon-21R, 3 μL of kb extender and 1 μL of Platinum Taq polymerase were added to a final volume of 50 μL. Amplification was done at 94°C for 2 min, 94°C for 30 sec, 53°C for 30 sec, 72°C for 2 min for 50 cycles with a final extension for 10 min at 72°C. PCR product was purified with the Promega gel and PCR cleanup kit (Promega, Madison, WI) and was submitted to the Eurofins genomic sequencing facility (Louisville, KY). Each reaction was split into 4 tubes and for sequencing with primers KIT-exon-8F, KIT-exon-15F, KIT-exon-21R and KIT-exon-16R.

Saturation mutagenesis was also performed starting with the primary activation loop mutant D816V. To perform saturation mutagenesis, Ba/F3 mutant KIT D816V cells were treated with ENU for 18 hr. Cells were washed several times, and then allowed to recover for 7 days, before adding to 96-well plates in the presence of compound for 28 days. Wells exhibiting outgrowth were expanded for DNA sequencing.

Mouse Xenograft Models

For the GIST T1 xenograft study, female nude mice (Hsd:Athymic Nude-Foxn1^{nu}; Envigo; 6-7 weeks old) were inoculated subcutaneously in the right high axilla with five million cells in Dulbecco's Phosphate Buffered Saline mixed with an equal volume of Matrigel. When tumor burdens reached 117 mm^3 on average on day 10, mice were randomly assigned into groups such that the mean tumor burden for all groups was within 10% of the overall mean tumor burden for the study population. Groups were treated on days 10-27 as follows: Vehicle control diet (n=8); ripretinib formulated into the mouse diet to achieve approximately 100 mg/kg/day of ripretinib (n=10); or ripretinib formulated into the mouse diet to achieve approximately 25 mg/kg/day of ripretinib (n=10). On Day 27, all animals were placed on control diet to monitor tumor regrowth.

For the GIST PDX KIT exon 11 deletion / exon 17 Y823D model, female NOD-SCID mice (Harlan Laboratories; 6-7 weeks old) were inoculated subcutaneously in the right flank with 100,000 viable cells in PBS mixed with an equal volume of Cultrex ECM. After 97 days, when tumor burdens reached 177 mm^3 on average, mice were randomly assigned into groups. Groups were treated for 28 days as follows: Vehicle control (20% Captisol, 0.4% hydroxypropylmethylcellulose and 25 mM $NaPO_4$, pH 2.0) PO, BID (n=10); ripretinib 100 mg/kg PO, QD (n=10); and ripretinib 50 mg/kg PO, BID (n=10). Dosing formulations were prepared once weekly and stored in the dark at 4°C. Dosing ended on day 28, and animals were monitored for tumor regrowth. For measurements of levels of phosphorylation of KIT and downstream signaling, mice were inoculated as above. On day 92, when when tumor burdens reached 240 mm^3 on average, mice were randomly assigned into groups (n=3). Tumors were collected from mice at 2 hr post dose on day 5. Harvested tumors were flash frozen in liquid N_2 and powdered. Tumor samples were processed as described in the western blot assay methods, with the following modifications. RIPA lysis buffer (Pierce, Rockford, IL) containing protease and phosphatase inhibitors was added to frozen tumor powder (~25-100 mg). Samples were then vortexed vigorously and placed on ice for 30 min, during which samples were mixed several more times. Protein was quantified using a bicinchoninic acid (BCA) Protein Assay (Pierce, Rockford, IL), using BSA as a standard.

For the P815 allograft model, female BALB/c nude mice (BALB/cOlaHsd-Foxn1^{nu}; Charles River Laboratories; 7-8 weeks old) were inoculated subcutaneously in the right high axilla with one million cells. When tumor burdens reached 84 mm^3 on average on day 5, mice were randomly assigned into groups such that the mean tumor burden for all groups was within 10% of the overall mean tumor burden for the study population. Groups were treated as follows: Vehicle control diet (n=10); ripretinib formulated into the mouse diet to achieve approximately 100 mg/kg/day of ripretinib (n=10); or ripretinib formulated into the mouse diet to achieve approximately 25 mg/kg/day of ripretinib (n=10).

For the HMC1.2 xenograft model, female nude mice (Hsd:Athymic Nude-Foxn1^{nu}; Envigo; 5-6 weeks old) were inoculated subcutaneously in the right high axilla with one million cells. When tumor burdens reached 157 mm^3 on average on day 10, mice were randomly assigned into groups such that the mean tumor burden for all groups was within 10% of the overall mean tumor burden for the study population. Groups were treated as follows: Vehicle control diet (n=10); ripretinib formulated into the mouse diet to achieve approximately 100 mg/kg/day of ripretinib (n=10); or ripretinib formulated into the mouse diet to achieve approximately 25 mg/kg/day of ripretinib (n=10).

For the H1703 xenograft model, female nude mice (Hsd:Athymic Nude-Foxn1^{nu}; Envigo; 6-7 weeks old) were inoculated subcutaneously in the right high axilla with five million cells in Dulbecco's Phosphate Buffered Saline mixed with an equal volume of Matrigel, using a 27 gauge needle and syringe. When tumor burdens reached 137 mm^3 on average on day 11, mice were randomly assigned into groups such that the mean tumor burden for all groups was within 10% of the overall mean tumor burden for the study population. Groups were treated on days 11-43 as follows: Vehicle control diet (n=10); ripretinib formulated into the mouse diet to achieve approximately 100 mg/kg/day of ripretinib (n=10); or ripretinib formulated into the mouse diet to achieve approximately 25 mg/kg/day of ripretinib (n=10). On Day 43, all animals were placed on the control diet to monitor tumor regrowth.

For the GIST T1 xenograft mouse pharmacokinetic/pharmacodynamic model, female nude mice (Crl:NU-Foxn1^{nu}; Charles River; 8-9 weeks old) were inoculated subcutaneously high in the right axilla with five million cells in serum free media mixed with an equal volume of Matrigel. For the time course study, when tumor burdens reached 237 mg on average on day 15, mice were randomly assigned into groups and were treated with single oral doses as follows: 0.4% hydroxypropylmethylcellulose vehicle control (n=4); ripretinib at 50 mg/kg (n=28); or ripretinib at 25 mg/kg (n=28). At 2 hr post dose for vehicle and 2, 4, 6, 8, 12, 18, and 24 hr post dose for ripretinib, whole blood was collected via cardiac puncture for plasma and tumors were excised, frozen in liquid N_2, and powdered. For the dose response study, when tumor burdens reached 264 mg on average on day 32, mice were treated with single oral doses as follows: 0.4% hydroxypropylmethylcellulose vehicle control (n=4); ripretinib at 100, 50, 25, 12.5, and 6.25 mg/kg (n=4/dose). At 2 hr post dose, whole blood was collected via cardiac puncture for plasma and tumors were excised, frozen in liquid N_2, and powdered.

Plasma samples on dry ice were sent for pharmacokinetic analysis to Xenometrics, LLC (Stilwell, KS). Tumor samples on dry ice were processed as described in the western blot assay methods, with the following modifications. RIPA lysis buffer (Pierce, Rockford, IL) containing protease and phosphatase inhibitors was added to frozen tumor powder (~25-100 mg). Samples were then vortexed vigorously and placed on ice for 30 min, during which samples were mixed several more times. Protein was quantified using a bicinchoninic acid (BCA) Protein Assay (Pierce, Rockford, IL), using BSA as a standard.

Ripretinib Phase 1 Study

An open label, nonrandomized, First-in-Human, phase 1, dose-escalation study with ripretinib in advanced or metastatic cancer patients with a focus on GIST (NCT02571036) was initiated to define the safety, MTD, pharmacokinetics, pharmacodynamics, and preliminary antitumor activity of ripretinib. Following the determination of the recommended phase 2 dose, an expansion cohort was started at 150 mg QD. Tumor assessment was done by CT scans every 4-week cycles per local assessment. For pharmacodynamics assessments in GIST patients, plasma samples were taken from patients to extract cell-free DNA, or cfDNA, which is DNA that is freely circulating in the bloodstream and not necessarily originating from a tumor. cfDNA was analyzed to identify the type and amount of KIT or PDGFRA mutations in the cfDNA that originated from tumors, which is known as circulating tumor DNA, or ctDNA.

ctDNA analysis protocol: 10 mL blood samples were collected in Streck cell-free DNA BCT® tubes and processed to plasma per manufacturing instructions. DNA extracted from plasma was analyzed using Guardant360 (Guardant Health, Inc.). Plasma drug levels were determined at KCAS Bioanalytical Services (Shawnee, KS). The studies were reviewed and approved by the institutional review boards at the University of Texas MD Anderson Cancer Center and Princess Margaret Cancer Centre. Written informed consent was obtained from all patients before study entry. Key eligibility criteria for adult patients ($\geq$18 years of age) with advanced refractory cancers (KIT/PDGFRA mutated) with a focus on GIST were ECOG performance status of 0 to 2 and adequate end organ function. Prior treatment with KIT/PDGFRA inhibitors was allowed.

QUANTIFICATION AND STATISTICAL ANALYSIS

Enzyme and cell data are represented as mean ± SD. Tumor burden and body weight change data are represented as mean ± SEM.

DATA AND SOFTWARE AVAILABILITY

The accession number for the X-ray crystal structure reported in this paper is PDB: 6mob.

ADDITIONAL RESOURCES

Ripretinib (DCC-2618) is being evaluated in a Phase 1 dose-escalation and expansion study. The two patients described in this paper were enrolled in this Phase 1 trial: https://clinicaltrials.gov/show/NCT02571036.

Ripretinib is also being evaluated in two Phase 3 trials: INVICTUS, a randomized placebo-controlled trial in 4th line and 4th line plus GIST patients: https://clinicaltrials.gov/show/NCT03353753, and INTRIGUE, a randomized 2nd line GIST trial evaluating ripretinib versus sunitinib: https://clinicaltrials.gov/show/NCT03673501.

Cancer Cell, Volume *35*

Supplemental Information

Ripretinib (DCC-2618) Is a Switch Control Kinase Inhibitor of a Broad Spectrum of Oncogenic and Drug-Resistant KIT and PDGFRA Variants

Bryan D. Smith, Michael D. Kaufman, Wei-Ping Lu, Anu Gupta, Cynthia B. Leary, Scott C. Wise, Thomas J. Rutkoski, Yu Mi Ahn, Gada Al-Ani, Stacie L. Bulfer, Timothy M. Caldwell, Lawrence Chun, Carol L. Ensinger, Molly M. Hood, Arin McKinley, William C. Patt, Rodrigo Ruiz-Soto, Ying Su, Hanumaiah Telikepalli, Ajia Town, Benjamin A. Turner, Lakshminarayana Vogeti, Subha Vogeti, Karen Yates, Filip Janku, Albiruni Ryan Abdul Razak, Oliver Rosen, Michael C. Heinrich, and Daniel L. Flynn

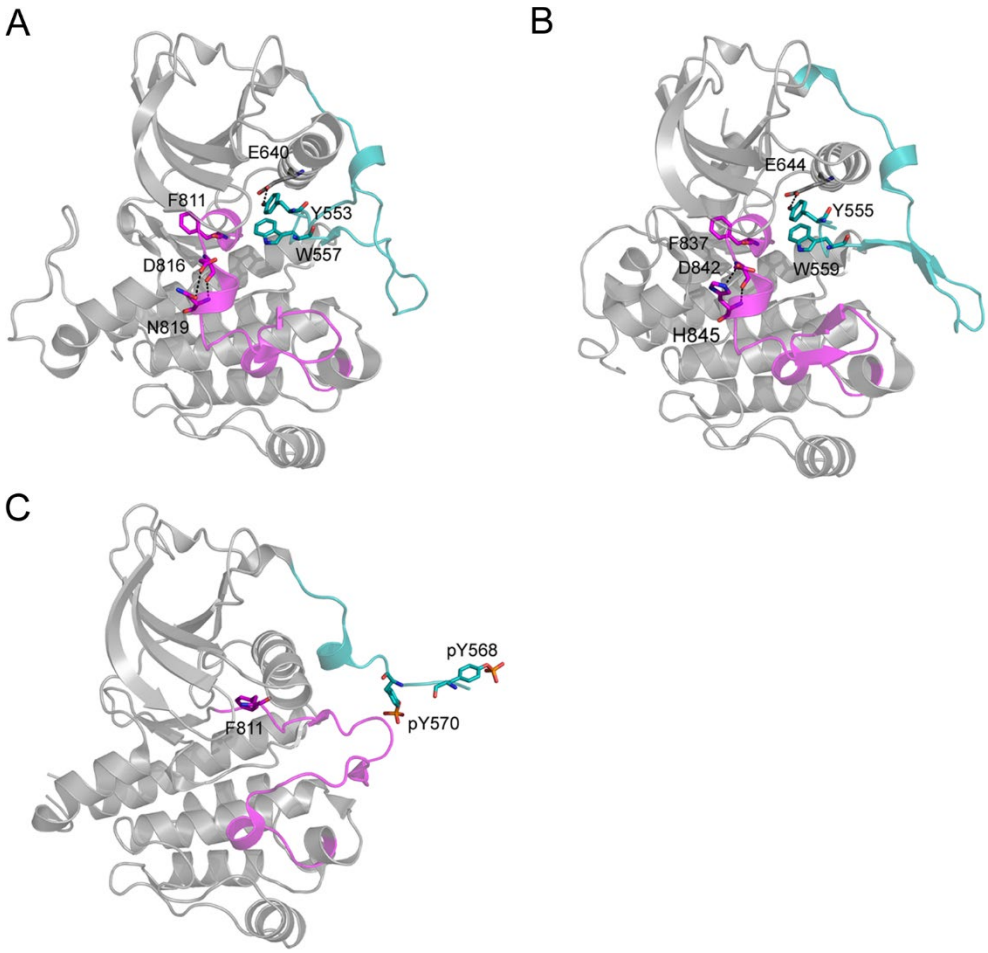

Figure S1. X-ray crystal structures of WT KIT and PDGFRA in their inactive Type II states or active Type I state, Related to Figure 1

(A) Unphosphorylated WT KIT, with activation loop (AL) switch (magenta) and inhibitory JMD switch (cyan) bound in the autoinhibited conformation. **(B)** Unphosphorylated WT PDGFRA, with AL switch (magenta) and inhibitory JMD switch (cyan) bound in the autoinhibited conformation. **(C)** JMD switch phosphorylated KIT, with AL switch (magenta) and inhibitory JMD switch (cyan) in the active conformation.

Table S1. Data collection and refinement statistics, Related to Figure 1

Crystal	204905d1
Beamline	CLS 081D-1
Space Group	*P*4(3)2(1)2
Unit Cell	
a (Å)	80.699
b (Å)	80.699
c (Å)	145.02
alpha	90
beta	90
gamma	90
Model Contents	
Protein	2488
Waters	311
HET groups	89
Data Collection:	
Resolution (Å)	1.8
High res. shell	1.86-1.80
Completeness (%)	96.5%
High res. shell	98.4%
Wilson B ($Å^2$)	25.3
R_{sym}	0.056
High res. shell	0.490
I/Sigma	24.7
last	3.5
Refinement:	
Resolution (Å)	1.8
rms_deviations	
bonds (Å)	0.015
angles (°)	1.489
R_{work}	18.3
R_{free}	21.0

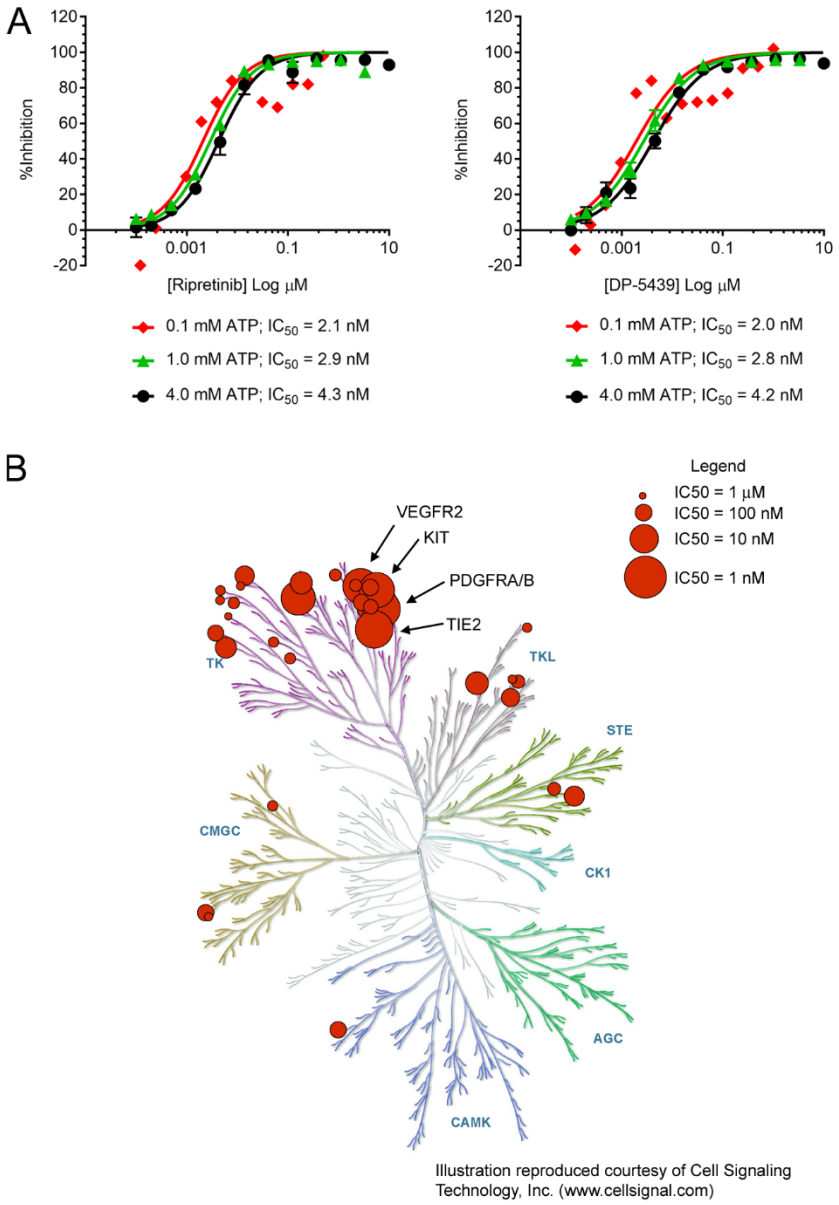

Figure S2. The effect of ATP on KIT inhibition and a kinome tree diagram for ripretinib, Related to Table 1

(A) Ripretinib and DP-5439 inhibition of WT KIT kinase at 0.1 mM, 1 mM, and 4 mM ATP. **(B)** For the kinome tree, a composite of enzyme and cellular kinase phosphorylation data was used. The size of the red circle corresponds to the IC_{50} value obtained. No circles are plotted for kinases with IC_{50} > 1 µM.

Table S2. Competitive binding data to KIT and PDGFRA, and inhibition of KIT mutants at 10 μM ATP, Related to Table 1

Competitive binding assay	Ripretinib	DP-5439	Activity assay at 10 μM ATP	Ripretinib	DP-5439
	K_d (nM)			IC_{50} (nM)	
KIT	7.8	4.8	KIT	16	7
KIT(V559D)	8.8	14	KIT (Δ557-558)	<0.1	<0.1
KIT(V559D/V654A)	33	57	KIT (V559A)	0.09	0.08
KIT(V559D/T670I)	25	31	KIT (V559D)	0.17	0.11
KIT(L576P)	24	27	KIT (V560G)	0.53	0.13
KIT(D816H)	53	37	KIT (K642E)	1.2	0.75
KIT(D816V)	13	18	KIT (V654A)	39	42
KIT(A829P)	11	33	KIT (T670I)	3.6	1.1
KIT-autoinhibited	1200	960	KIT (D816E)	0.27	0.17
PDGFRA	21	11	KIT (D816F)	0.29	0.21
			KIT (D816H)	0.34	0.22
			KIT (D816I)	0.26	0.17
			KIT (D816V)	0.25	0.16
			KIT (D816Y)	0.42	0.26
			KIT (D820E)	0.2	0.13
			KIT (D820Y)	0.15	0.11
			KIT (Y823D)	0.14	0.1
			KIT (V560G/D816V)	0.12	0.09
			KIT (V560G/N822K)	0.15	0.11

Table S3. Kinase profile, Related to Table 1

IC_{50} Range	Kinases inhibited by ripretinib in enzymatic assays
1 - 10 nM	KIT (3 nM), PDGFRA (4 nM), BRAF (7 nM)[a], DDR2 (4 nM)
10 - 100 nM	CSF1R (15 nM)[a], EPHB2 (70 nM), LCK (50 nM), PDGFRB (38 nM)[a], RAF1 (21 nM)[a], TAOK2 (60 nM), TIE2 (61 nM)[a], TRKA (40 nM), ZAK (35 nM)
100 - 1000 nM	ARAF (391 nM), EPHA2 (351 nM), EPHA3 (550 nM), EPHA4 (315 nM), EPHA5 (462 nM), EPHA8 (410 nM), EPHB1 (617 nM), FGFR1 (283 nM), FLT1 (290 nM), FLT3 (180 nM), FLT4 (130 nM), HIPK4 (394 nM), LOK (245 nM), LYN (130 nM), MELK (360 nM), MLK1 (480 nM), MLK3 (553 nM), MYLK2 (120 nM), p38a (615 nM), p38b (120 nM), TAOK3 (385 nM), VEGFR2 (120 nM)[a], YES (723 nM)

[a]See cellular kinase data in Table S4.

Table S4. Inhibition of kinase phosphorylation in cell-based assays, Related to Table 1

	HUVEC (VEGFR2)	H1703 (PDGFRA)	REN (PDGFRB)	HUVEC (TIE2)	THP-1 (CSF1R)	MV-4-11 (FLT3-ITD)	A375 (BRAF V600E)	HCT-116 (BRAF/CRAF)
	IC_{50} (nM)							
Ripretinib	3	6	4	2	123	57	230	580

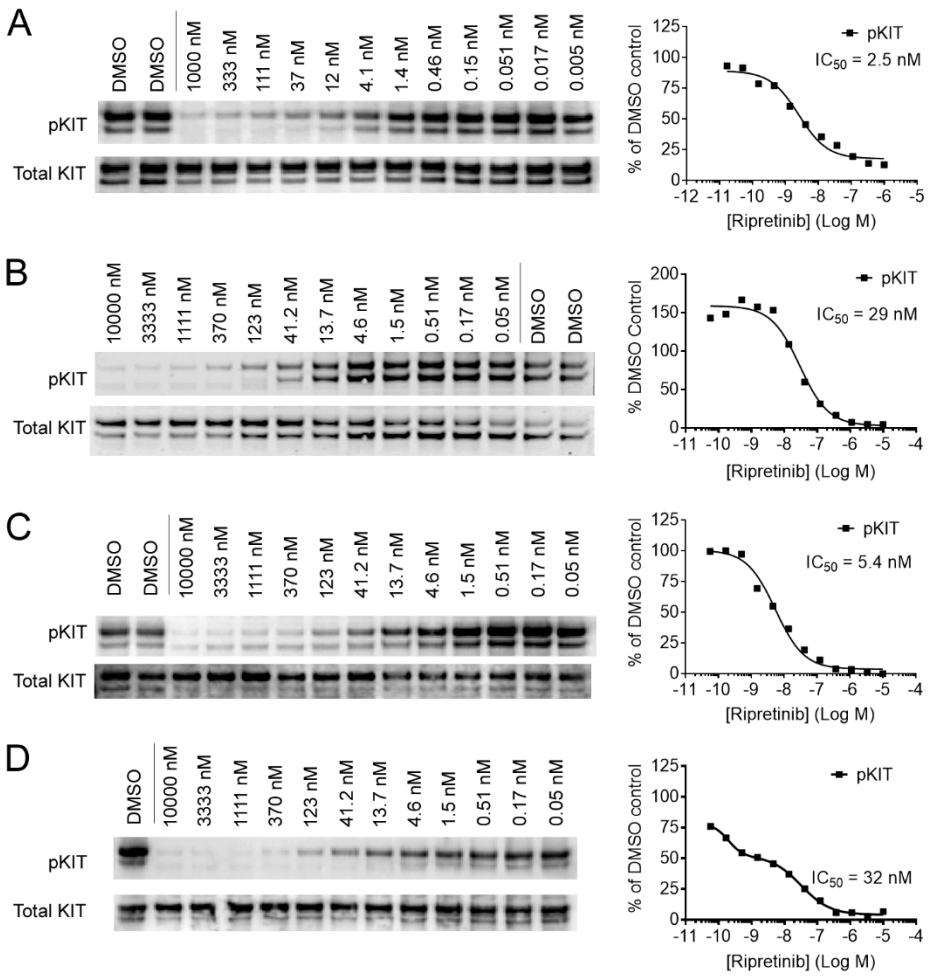

Figure S3. **Inhibition of KIT phosphorylation in GIST patient cell lines, Related to Figure 2**

(A) Representative dose response Western blot of ripretinib in GIST T1 cells (primary exon 11 deletion). Levels of phosphorylated KIT (Y719) and total KIT are shown. **(B)** GIST 882 cells (primary exon 13 K642E mutation). **(C)** GIST 430 cells (primary exon 11 deletion / secondary exon 13 V654A mutation). **(B)** GIST 48 cells (primary exon 11 V560D mutation / secondary exon 17 D820A mutation). The secondary mutation is heterozygous and a biphasic curve is observed. The IC_{50} value corresponding to the double mutant is shown.

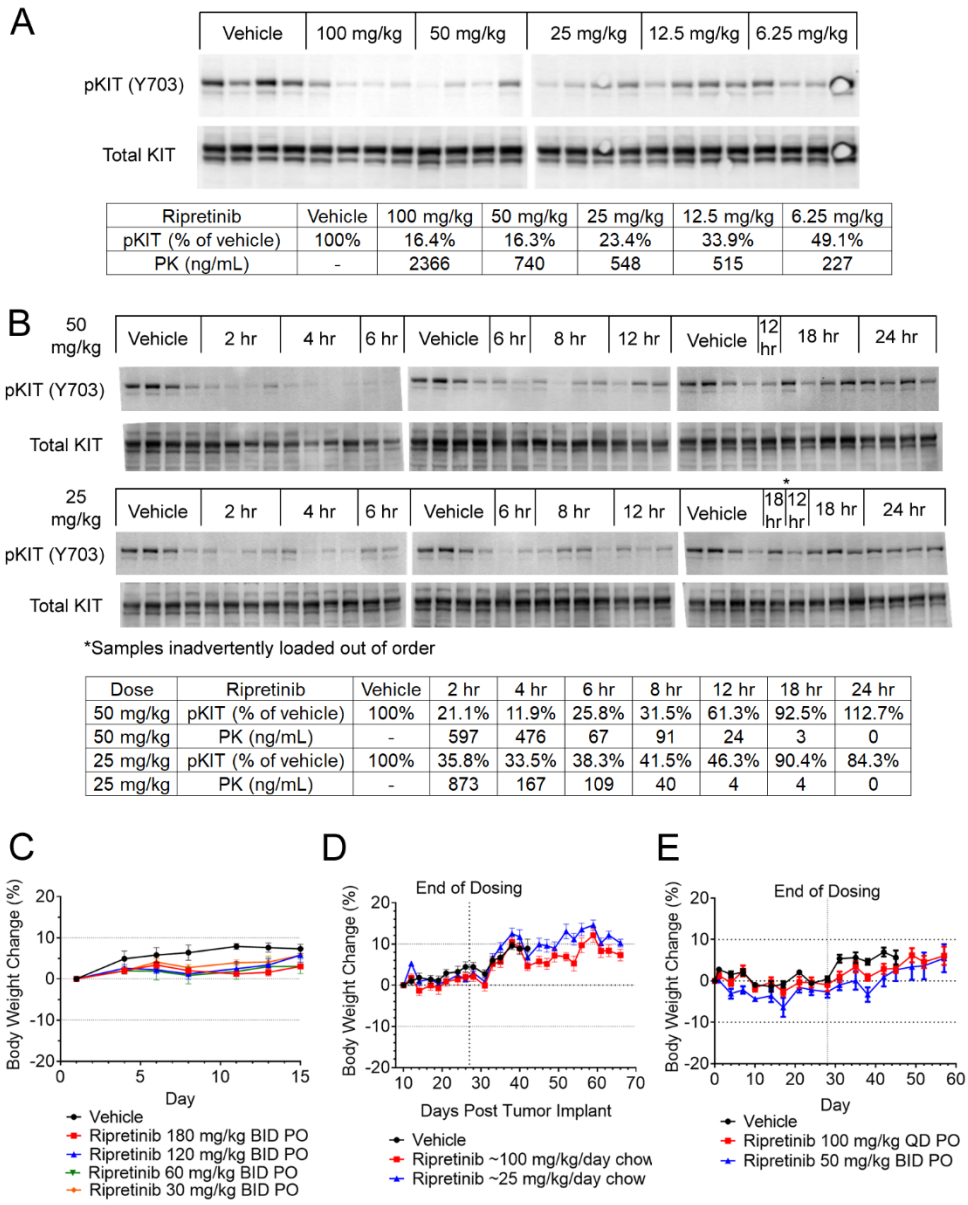

Ripretinib	Vehicle	100 mg/kg	50 mg/kg	25 mg/kg	12.5 mg/kg	6.25 mg/kg
pKIT (% of vehicle)	100%	16.4%	16.3%	23.4%	33.9%	49.1%
PK (ng/mL)	-	2366	740	548	515	227

Dose	Ripretinib	Vehicle	2 hr	4 hr	6 hr	8 hr	12 hr	18 hr	24 hr
50 mg/kg	pKIT (% of vehicle)	100%	21.1%	11.9%	25.8%	31.5%	61.3%	92.5%	112.7%
50 mg/kg	PK (ng/mL)	-	597	476	67	91	24	3	0
25 mg/kg	pKIT (% of vehicle)	100%	35.8%	33.5%	38.3%	41.5%	46.3%	90.4%	84.3%
25 mg/kg	PK (ng/mL)	-	873	167	109	40	4	4	0

Figure S4. Pharmacokinetic/pharmacodynamic data of ripretinib in the GIST T1 xenograft model, and body weight changes in xenograft and MTD studies, Related to Figure 3

(A) Dose response study of 100, 50, 25, 12.5, and 6.25 mg/kg ripretinib, with tumor and plasma samples harvested at 2 hr post single oral dosing. Levels of pKIT (Y703) and plasma PK of drug represent mean data from four mice each. **(B)** Time course study of 50 and 25 mg/kg ripretinib, with tumor and plasma samples harvested at 2, 4, 6, 8, 12, 18, and 24 hr post single oral dosing. **(C)** Body weight change in the 14-day mouse MTD study. Mice were dosed day 1 through day 14. Data are represented as mean ± SEM. **(D)** Body weight change in the GIST T1 xenograft tumor model. Mice were treated with ripretinib formulated diet from Day 10 to Day 27. Data are represented as mean ± SEM. **(E)** Body weight change in the GIST PDX model. Mice were dosed on Day 0 through Day 28. Data are represented as mean ± SEM.

Table S5. Summary PK data for mouse and rat studies, and two patients treated with ripretinib, Related to Figure 4

PK Parameters	Mouse	Mouse	Rat	Patient 1	Patient 2
Study	Single dose PK/PD 50 mg/kg	2-week MTD 180 mg/kg BID	4-week toxicology study NOAEL 300 mg/kg/day	Phase 1 Study 50 mg BID	Phase 1 Study 150 mg BID
C_{max} (ng/mL)	597-893[a]	2,290[a]	3,990[b]	1,820[b]	7,880[b]
C_{min} (ng/mL)	0[a]	n.a.	143[b]	1,120[b]	6,550[b]
AUC 0-24hr (ng*h/mL)	~5,000[a]	n.a.	31,890[b]	n.a.	n.a.

[a]Data for ripretinib is shown. Metabolite DP-5439 was not measured. [b]PK parameters include analysis of both parent ripretinib and metabolite DP-5439. n.a. = not available.